JCI The Journal of Clinical Investigation

CC17 Group B *Streptococcus* exploits integrins for neonatal meningitis development

Romain Deshayes de Cambronne, … , Claire Poyart, Julie Guignot

J Clin Invest. 2021. https://doi.org/10.1172/JCI136737.

Research In-Press Preview Infectious disease Microbiology

Graphical abstract

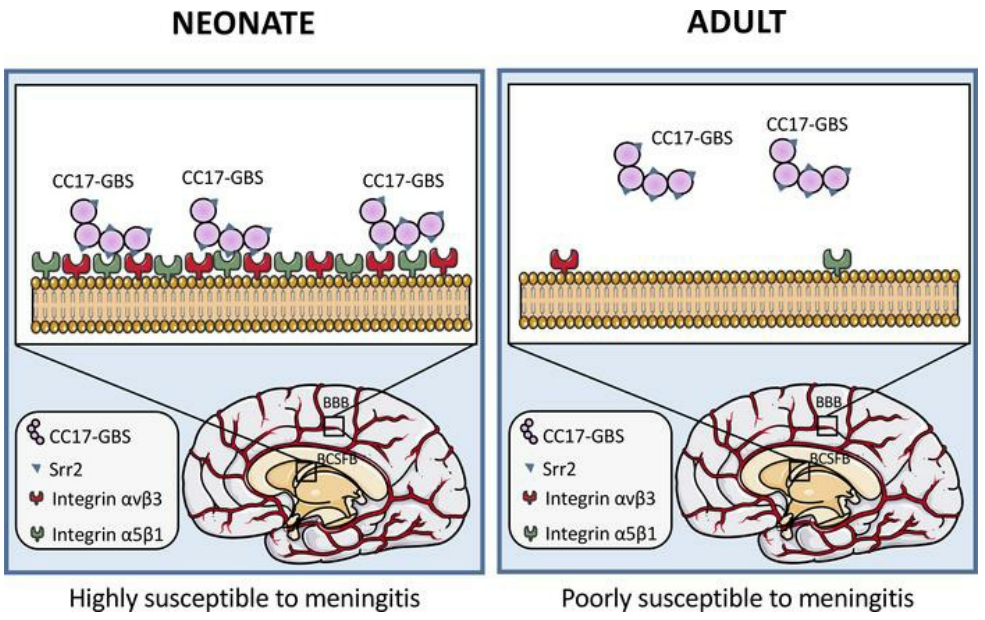

CC17 Group B *Streptococcus* exploits integrins for neonatal meningitis development

Romain Deshayes de Cambrone[1], Agnès Fouet[1], Amandine Picart[1], Anne-Sophie Bourrel[1,2], Cyril Anjou[1], Guillaume Bouvier[4], Cristina Candeias[1], Abdelouhab Bouaboud[1], Lionel Costa[1], Anne-Cécile Boulay[5], Martine Cohen-Salmon[5], Isabelle Plu[6], Caroline Rambaud[7], Eva Faurobert[8], Corinne Albigès-Rizo[8], Asmaa Tazi[1,2,3], Claire Poyart[1,2,3], Julie Guignot[1*]

[1]Université de Paris, Institut Cochin, INSERM, U1016, CNRS, UMR8104, F-75014 Paris, France; [2]Hôpitaux Universitaires Paris Centre, Cochin, Assistance Publique Hôpitaux de Paris, France; [3]Centre National de Référence des Streptocoques, France; [4]Structural Bioinformatics Unit, Department of Structural Biology and Chemistry, Institut Pasteur, CNRS UMR3528, C3BI, USR3756 Paris, France; [5]Center for Interdisciplinary Research in Biology (CIRB), Collège de France, CNRS UMR7241, INSERM U1050, PSL Research University, Paris, France; [6]Sorbonne Université /Département de neuropathologie Raymond Escourolle - Hôpital Pitié-Salpêtrière - Assistance Publique-Hôpitaux de Paris, France; [7]Université de Versailles Saint Quentin en Yvelines (Université Paris-Saclay)/Service d'anatomie-pathologique et médecine légale, Hôpital Raymond Poincaré, Garches, France; [8]INSERM U1209, CNRS UMR 5309, Institute for Advanced Biosciences, France/Université Grenoble Alpes, F-38700 La Tronche, France.

***** To whom correspondence should be addressed: julie.guignot@inserm.fr

ORCID number: 0000-0001-8890-4028. Tel: + 33 1 40 51 64 13; Fax: + 33 1 40 51 64 54.

Institut Cochin, 22 rue Méchain 75014 Paris, France.

CONFLICT OF INTEREST:

The authors have declared that no conflict of interest exists.

KEYWORDS: Srr2, CC17, *Streptococcus agalactiae*, Group B Streptococcus, meningitis, integrin, neonatal susceptibility, blood brain barrier (BBB)

ABSTRACT

Group B *Streptococcus* (GBS) is the major cause of human neonatal infections. A single clone, designated CC17-GBS, accounts for more than 80% of meningitis cases, the most severe form of the infection. However, the events allowing blood-borne GBS to penetrate the brain remain largely elusive. In this study, we identified the host transmembrane receptors $\alpha5\beta1$ and $\alpha v\beta3$ integrins as the ligands of Srr2, a major CC17-GBS specific adhesin. Two motifs located in the binding region of Srr2 were responsible for the interaction between CC17-GBS and these integrins. We demonstrated, in a blood-brain barrier cellular model, that both integrins contributed to the adhesion and internalization of CC17-GBS. Strikingly, both integrins were overexpressed during the post-natal period in the brain vessels of the blood-brain and blood-cerebrospinal fluid barriers and contributed to the juvenile susceptibility to CC17-meningitis. Finally, blocking these integrins decreased CC17-GBS crossing into the juvenile mice central nervous system in an *in vivo* model of meningitis.

Our study demonstrates that CC17-GBS exploits integrins for crossing the brain vessels leading to meningitis. Importantly, it provides host molecular insights into neonate's susceptibility to CC17-GBS meningitis, thereby opening new perspectives for therapeutic and prevention strategies of GBS-elicited meningitis.

INTRODUCTION

In the early 1950's, due to the massive utilization of tetracyclines, *Streptococcus agalactiae* (Group B *Streptococcus*, GBS) emerged worldwide as the most significant pathogen causing severe neonatal invasive infections (1). This commensal bacterium, which is found in the intestine and the genital tract of 11 to 22% of healthy humans (2), is responsible for two syndromes in neonates, the early-onset disease (EOD) which occurs within the first 48 hours after birth in 90% of the cases, and the late-onset disease (LOD) which occurs between 7 and 89 days of life (3). EOD results from mother-to-child vertical transmission of the bacterium through the inhalation of GBS-contaminated amniotic fluid or vaginal secretions during delivery. EOD often manifests by bloodstream infections that are complicated by meningitis in 15 to 30% of the cases (4). The onset of LOD remains largely unknown, although recent studies argue for the co-existence of both *intrapartum* and post-natal transmission routes and for a gastrointestinal portal of entry (5-7). Meningitis is common during LOD, up to 50% of the cases, mainly due to one particular GBS clone almost exclusively of capsular serotype III and belonging to the clonal complex (CC) 17. Overall, as reported by worldwide epidemiological studies, the so-called hypervirulent CC17-GBS is responsible for 80% to 95% of the cases of neonatal GBS-elicited meningitis, both syndromes combined, highlighting a strong meningeal tropism (4, 8-11).

The critical step for meningitis development is the transmigration of blood-borne-GBS into the central nervous system (CNS). Brain is normally protected by physiological barriers that separate the blood from the brain parenchyma or the cerebrospinal fluid. Brain microvascular endothelial cells and choroid plexus epithelial cells that compose the blood-brain barrier (BBB) and the blood-cerebrospinal fluid barrier (BCSFB), respectively, are both characterized by the presence of tight junctions that are crucial for the maintenance of the barrier function. To penetrate those barriers, blood-borne bacteria can either use a transcellular mechanism that requires pathogen internalization and/or a paracellular mechanism that requires tight junction disruption. Alternatively bacteria can use phagocytes as Trojan horse (12). GBS has been described to be internalized in

cerebral endothelial cells, but also to inhibit tight junction proteins expression, suggesting that GBS could use trans and/or paracellular mechanisms to penetrate the brain (13, 14).

CC17 strains were shown to display higher adherence properties to brain endothelial cells compared to non-CC17 strains (15). Two CC17-GBS specific surface adhesins, Srr2 and HvgA, account for the increased binding of CC17-GBS to brain endothelial cells compared to non-CC17 strains and contribute to BBB crossing in *in vivo* model of meningitis (15, 16). However, how these proteins contribute to brain barrier crossing at the molecular level is currently unknown.

Here, we demonstrate that Srr2 directly and specifically binds to integrins $\alpha5\beta1$ and $\alpha v\beta3$, thereby contributing to the adhesion and invasion of brain endothelial cells and to the crossing of brain barriers leading to meningitis development.

Most importantly, we show that these receptors are overexpressed during the postnatal period in brain vessels, arguing for CC17-GBS increased invasiveness of the CNS in neonates.

RESULTS

The Binding Region (BR_{Srr2}) of the Srr2-CC17 specific adhesin interacts with $\alpha5\beta1$ and $\alpha v\beta3$ integrins

In contrast to HvgA for which no molecular ligand has been identified, Srr2 contains a fibrinogen-binding site within the region, termed Binding Region (BR_{Srr2}), involved in CC17-GBS adhesion to a variety of host cells (16-19). A Srr2-homologous protein, designated Srr1, which also possesses a fibrinogen binding site in its Binding Region (BR_{Srr1}), is expressed by non-CC17 GBS isolates. Although Srr2 and Srr1 have a similar structure, they display only 37% amino–acid sequence identity in their Binding Regions (Fig.1A). Looking in BR_{Srr2} for binding motifs which could account for the hyper-adhesion phenotype properties of CC17-GBS to host cell, we identified by sequence analysis an Arg-Gly-Asp (RGD) and a Ser-Asp-Val (SDV) motifs which are absent from BR_{Srr1} (Fig.1A). These two motifs are known to allow integrin recognition (20, 21). Integrins are transmembrane heterodimeric receptors composed of one α and one β subunit that combine to form up to 24 different integrins. While the SDV motif has been recently identified to be specific of $\alpha v\beta3$, the RGD motif is recognized by a number of different integrins (22, 23). We therefore focused our study on $\alpha5\beta1$ and $\alpha v\beta3$ integrins known to recognize RGD or SDV motifs and, to be expressed by brain endothelial cells as CC17 strains are highly correlated to meningitis (24, 25).

We therefore compared the interaction of BR_{Srr2} and BR_{Srr1} with $\alpha5\beta1$ and $\alpha v\beta3$ integrins. We first measured by immunoblotting the direct binding of BR_{Srr2} and BR_{Srr1} to immobilized recombinant soluble human integrins $\alpha5\beta1$ and $\alpha v\beta3$. Intense signals were obtained with BR_{Srr2} where $\alpha5\beta1$ and $\alpha v\beta3$ integrins were spotted, but not where ICAM1, another transmembrane protein, was spotted, indicating that BR_{Srr2} binds to recombinant human $\alpha5\beta1$ and $\alpha v\beta3$ integrins (Fig. 1B). In contrast, weak signals were observed when BR_{Srr1} was assayed in the same conditions with $\alpha5\beta1$ and $\alpha v\beta3$ integrins (Fig. 1B).

The interaction between BR_{Srr2} and human $\alpha5\beta1$ and $\alpha v\beta3$ integrins was further confirmed by ELISA assays showing that recombinant human $\alpha5\beta1$ and $\alpha v\beta3$ integrins bind to immobilized BR_{Srr2} in a saturable and dose-dependent manner, whereas they failed to bind to BR_{Srr1} (Fig. 1C and 1D). As a control, ICAM1 bound neither to BR_{Srr2} nor to BR_{Srr1} (Fig. 1E). Moreover, no interaction was observed between the $\alpha5\beta1$ and $\alpha v\beta3$ integrins and HvgA, the other CC17-GBS specific adhesin (data not shown).

Integrin structure and ligand binding affinity are strongly affected by divalent cations concentrations (26). This property was confirmed for BR_{Srr2}-integrin interaction by ELISA assays in presence of $CaCl_2$ or $MnCl_2$. Addition of Ca^{2+} or Mn^{2+} totally abolished $\alpha5\beta1$ integrin binding to BR_{Srr2}, while Ca^{2+} strongly enhanced $\alpha v\beta3$ integrin binding to BR_{Srr2} (Fig. S2A and B). Last, the interaction between BR_{Srr1} and BR_{Srr2} with non-RGD recognizing integrins expressed by brain endothelial cells ($\alpha6\beta1$; $\alpha4\beta1$; $\alpha3\beta1$) and non-RGD recognizing integrins described to directly bind to GBS ($\alpha1\beta1$) were analyzed (24, 27). Interestingly, both BR_{Srr1} and BR_{Srr2} interacted with $\alpha6\beta1$; $\alpha4\beta1$; $\alpha3\beta1$ integrins, however this is not a general feature to all integrins as $\alpha1\beta1$ failed to bind both BR_{Srr1} and BR_{Srr2} (Fig. S3).

Altogether, our data show that $\alpha5\beta1$ or $\alpha v\beta3$ integrins are directly and specifically recognized by BR_{Srr2}.

$\alpha v\beta3$-*BR_{Srr2} interaction depends on the RGD and SDV motifs*

In order to test the role of the RGD and SDV motifs present on BR_{Srr2} in their interaction with integrins, mutated forms of BR_{Srr2} were produced in which the RGD or/and the SDV motifs were replaced by three alanines (Fig. S1B and C). The interaction between BR_{Srr2} mutated forms with integrins $\alpha v\beta3$ or $\alpha5\beta1$ was assessed by ELISA. RGD and/or SDV substitutions strongly affected

αvβ3 integrin binding (Fig. 2A), but not that with α5β1 integrin (Fig. 2B). No additive inhibition was observed when both motifs (RGD and SDV) were mutated (Fig. 2A).

The contribution of these motifs to integrin binding was further supported by competitive ELISA assays using synthetic peptides containing an RGD sequence (RGDS and RGDfV peptides) or an SDV sequence (P11 peptide) that are widely used to inhibit integrin recognition (20, 21). RGD and SDV peptides significantly inhibited αvβ3-BR_{Srr2} interaction in a dose-dependent manner, whereas they had no significant effect on α5β1- BR_{Srr2} interaction (Fig. 2C and 2D).

Altogether, these results demonstrate that the interaction of BR_{Srr2} with integrin αvβ3 requires both RGD and SDV motifs, whereas the interaction with integrin α5β1 is independent from these motifs.

BR_{Srr2} interaction with integrin α5β1 involves two other motifs

To identify BR_{Srr2} residues involved in α5β1 integrin recognition, we used the RaptorX webserver which enables, by combining co-evolution and deep learning, to predict residue - residue interactions (28). Using this approach, two putative motifs of interaction between BR_{Srr2} and α5β1 were identified (Fig. S4A and Fig. 2E). The first one is an FSVKI motif located in the N-terminal subdomain of BR_{Srr2} at position 362 and the second one is an ETYVI motif located in the C-terminal subdomain of BR_{Srr2} at position 496 (Fig. 2E and 2F). These two motifs are absent from the BR_{Srr1} sequence. To address the role of these two motifs in the interaction with integrin α5β1, we first addressed the binding capacities of BR_{Srr2} subdomains containing these motifs. The N-terminal and C-terminal subdomains of BR_{Srr2} containing either motif were produced, and equimolar amount of full length BR_{Srr2}, N-terminal and C-terminal domains were used to perform ELISA binding assays. The α5β1 integrin displayed a similar capacity to bind to all three forms of BR_{Srr2} (Fig. 2G) indicating the presence of at least one binding motif on each of BR_{Srr2} sub-domains.

We next generated mutated forms of BR_{Srr2} in which the FSVKI or the ETYVI sequences were replaced by FAAAI and AAYAI, respectively (Fig. S1D and E) and the interaction with integrin

157 α5β1 was assessed by ELISA. While the mutation of the ETYVI motif affects the interaction with
158 α5β1 integrin only at the highest concentration, the mutation of the FSVKI motif significantly
159 reduced the binding to α5β1 integrin at most concentrations (Fig. 2H).
160 Altogether, we identified the FSVKI motif of BR_{Srr2} as required for α5β1 integrin recognition.
161 Besides, we demonstrated that BR_{Srr2} contains at least one other integrin α5β1 recognition motif
162 which is located in its C-terminal region but remains to be identified. Interestingly, when integrin
163 binding motifs were highlighted on BR_{Srr2}, we noticed that both αvβ3 binding motifs (RGD and
164 SDV) are localized on the same side of BR_{Srr2}, while α5β1 binding motif, FSVKI, is located on the
165 opposite side (Fig. S4B).

166

167 ***Human α5β1 integrin acts as a receptor for Srr2-expressing GBS in a simplified model of***
168 ***CHO cells***
169 To determine whether α5β1 and αvβ3 integrins are viable candidate-receptors for adhesion and/or
170 invasion of CC17-GBS, the binding of a CC17-GBS strain to a simplified model where cells
171 ectopically express human α5β1 or αvβ3 integrins was assessed. We infected the Chinese
172 Hamster Ovary (CHO) control cell line, which does not express endogenous β3 nor α5 integrin
173 subunits and which is therefore deficient for the expression of α5β1 and αvβ3 integrins (29), or
174 CHO cells stably transfected with plasmids encoding human α5β1 (CHO-α5β1), human αvβ3
175 (CHO-αvβ3) or human ICAM1 as a control (30-32).
176 Numerous CC17-GBS were observed adhering to CHO-α5β1 cells (Fig. 3A arrows) as compared
177 to non-transfected CHO or CHO-ICAM1 cells that were non-permissive for CC17 adhesion where
178 most streptococci were found unbound to cells (Fig. 3 A, arrow heads). Immunostaining with anti-
179 α5 antibody showed that CC17-GBS were almost exclusively associated to cells expressing
180 integrin α5β1, while very rare bacteria were associated with cells that had lost its expression (Fig.

3B). In addition, few CC17-GBS bacteria adhered to CHO-αvβ3 (Fig. 3A). However, only the adhesion to α5β1 expressing cells was statistically significant (Fig. 3C). We next analyzed the specificity of CC17-GBS interaction with α5β1 integrin by testing adhesion of a non-CC17 GBS strain (CC23) expressing the Srr1 surface protein to CHO transfected cells. The CC23 GBS strain did not show proficient adhesion to any CHO cell lines tested (Fig. 3C). Altogether, these results indicate that integrin α5β1 is an effective and specific host receptor for CC17-GBS.

To demonstrate that the binding to α5β1 integrin by CC17-GBS was dependent on Srr2, we tested the adhesion of CC17 Δ*srr2* derived strains. The adhesion of the Δ*srr2* mutant strain to CHO-α5β1 revealed a clear defect when compared to that of the isogenic wild type (WT) strain. Complementation of the Δ*srr2* mutant with a plasmid expressing BR_{Srr2} domain was sufficient to restore adhesion to WT level. In agreement with this result, adhesion of CC17-GBS to CHO-α5β1 was inhibited by anti-Srr2 antibody. Altogether, these data demonstrate that Srr2 is responsible for CC17-GBS adhesion to α5β1 integrin (Fig. 3D).

Finally, using a differential staining allowing to discriminate extracellular from intracellular streptococci, we were able to detect internalized CC17-GFP bacteria in CHO-α5β1 cells (Fig. 3E). Comparing invasion rates obtained with CHO-α5β1 and with untransfected cells, by CFU counting, indicated that α5β1 integrin also promotes CC17-GBS internalization in a Srr2-dependant manner (Fig. 3F).

In conclusion, our data demonstrate that Srr2 expression allows α5β1 integrin recognition promoting CC17-GBS adhesion and invasion in a simplified cellular model.

α5β1 and αvβ3 integrins promote the binding and invasion of CC17-GBS to cerebral endothelial cells

Blood-borne CC17-GBS must interact with the luminal face of cerebral endothelial cells to access CNS. Because integrins are known to be expressed on the luminal and abluminal faces of

endothelial cells (33-36), we addressed the role of integrins in a more physiological relevant model of cerebral endothelial cells. We previously showed that CC17-GBS display a hyper-adhesion phenotype on cerebral endothelial cells compared to non-CC17 GBS strains (15). Both CC17 specific adhesins HvgA and Srr2 contribute to the adhesion properties of CC17-GBS (15, 17). Therefore, we proposed to address the role of Srr2-integrin interaction in CC17-GBS adhesion to cells of the BBB. We first confirmed, using the human cerebral endothelial cell line hCMEC/D3, that CC17-GBS adheres, in a Srr2-dependent manner, more than the non-CC17 strain (CC23) (Fig. 4A). Since the expression of bacteria recognizing cellular receptors may change upon infection, we analyzed integrins expression. Expression of α5β1 and αvβ3 were not modified by infection with CC17-GBS for up to 3 hours neither at the transcriptional level (Fig. S5A and C) nor at the protein level (Fig. S5B and D). To investigate if $\alpha5\beta1$ and $\alpha v\beta3$ integrins could contribute to CC17 hyper-adhesion to brain endothelial cells, we performed competition experiments with soluble integrins. When CC17-GBS were pre-incubated with soluble human $\alpha5\beta1$ or $\alpha v\beta3$ integrins, CC17 adhesion to hCMEC/D3 was significantly reduced compared to that of the untreated control (Fig. 4B). No additive effect was observed when both $\alpha5\beta1$ and $\alpha v\beta3$ integrins were mixed. As a control, pre-incubation with soluble ICAM1 did not alter CC17-GBS adhesion. Neither $\alpha5\beta1$, nor $\alpha v\beta3$ integrins, nor ICAM1 soluble protein affected the adhesion of the Δ*srr2* mutant or that of non-CC17-GBS (Fig. 4B), indicating that the adhesion of CC17-GBS to hCMEC/D3 cells depends on Srr2-$\alpha5\beta1$ and Srr2-$\alpha v\beta3$ interactions.

To confirm the role of $\alpha5\beta1$ and $\alpha v\beta3$ integrins in CC17-GBS adhesion to hCMEC/D3, we silenced the integrins expression by transfecting endothelial cells with specific siRNAs. Because integrins are composed of one α chain and one β chain that combine to form heterodimers, we targeted the $\alpha5$ chain to silence $\alpha5\beta1$ and the $\beta3$ chain to silence $\alpha v\beta3$, a strategy which minimizes side effects on other integrins. The effect of siRNA-mediated silencing of α5 or β3 chains was efficient as evidenced by Western Blot analysis (Fig. 4C and D). When $\alpha5$ or $\beta3$ expression was silenced,

CC17-GBS adhesion was significantly reduced compared with scramble control-transfected cells. No additive effect was observed when both α5 and β3 were simultaneously silenced. In contrast, adhesion of the Δ*srr2* mutant strain or the non-CC17-GBS were not affected by α5 or β3 integrin silencing (Fig. 4E).

Finally, we investigated the contribution of Srr2-integrins interactions in cellular barrier crossing. Indeed, bacterial adhesion to brain endothelial cells is a prerequisite for the crossing of the BBB by either paracellular or transcellular mechanism. When brain microvascular endothelial cells were infected with the CC17 strain for 1 h, no obvious disruption of the ZO1 tight junction protein was observed (Fig. 4F). Furthermore, staining allowing to differentiate extracellular from intracellular bacteria revealed the presence of intracellular bacteria suggesting a transcellular passage (Fig. 4F). We therefore compared the invasion by a CC17-GBS to that of the Δ*srr2* and non-CC17-GBS strains (Fig. 4G). Invasion of the WT CC17 was higher than that of the other strains, demonstrating the existence of a Srr2- dependent invasion (Fig. 4G). We thus assayed the consequences of siRNA silencing of α5 or β3 expression on CC17-GBS internalization. Invasion level of CC17-GBS was significantly reduced in α5 and β3 silenced cells (Fig. 4H). In contrast, internalizations of the Δ*srr2* mutant and the non-CC17 GBS were unmodified (Fig. 4H). To analyze CC17-GBS internalization process in hCMEC/D3, and the putative involvement of signal transduction molecules involved in integrin signaling, we performed invasion assays in the presence of various inhibitors. The actin-depolymerizing agent (cytochalasin D), the cholesterol-depleting agent (methyl-β-cyclodextrin) and the dynamin-2 inhibitor (dynasore) inhibited CC17-GBS invasion. In contrast, the microtubule-depolymerizing agent (nocodazole), the PI3Kinase inhibitor (wortmannin) or the Akt inhibitor (MK22) had no effect (Fig. 4I).

Altogether, these results indicate that the Srr2 adhesin expressed by CC17-GBS uses α5β1 and αvβ3 integrins to promote the adhesion of CC17 strains on cerebral endothelial cells, leading to their internalization by a mechanism involving actin, dynamin-2 and lipid rafts.

α5β1 and αvβ3 integrins are overexpressed during the postnatal period

CC17-GBS are over-represented among GBS neonatal meningitis, accounting for more than 80% of the cases (4, 9, 11). In contrast, epidemiological data show that GBS is an uncommon cause of meningitis in adults and CC17 is only found in 21% of the cases (37, 38). Meningeal pathogens can enter the brain *via* the BBB and/or the BCSFB located in the choroid plexuses of the ventricular area (12). We therefore hypothesized that neonatal susceptibility to CC17-GBS meningitis might be correlated to the expression of α5β1 and αvβ3 integrins at the BBB/BCSFB level. To test this hypothesis, cerebral blood vessels from neonatal and adult rats were purified and the expression of α5β1 and αvβ3 was assessed by immunofluorescence staining and Western Blot analysis. A striking intense α5 integrin staining was observed on brain vessels from pups while adult brain vessels displayed a much less intense staining (Fig. 5A). Overexpression of α5 integrin in neonatal brain vessels was confirmed by Western Blot analysis (Fig. 5B). While no β3 expression was detected on adult brain vessels, either by immunofluorescence or by Western Blot, a faint but easily detectable β3 expression was observed in brain vessels from pups rats (Fig. 5B and 5C). These results indicate that α5β1 and αvβ3 integrins are overexpressed in rat brain vessels during the neonatal period.

Choroid plexuses are composed of blood vessels which are different from those of the BBB, and of stroma and choroid epithelial cells that form the BCSFB (39). Therefore, choroid plexus tissues from the 4th ventricle (CP4V) or the lateral ventricles (CPLV) were collected and analyzed for α5 and β3 expression. α5 integrin was found overexpressed in rats pups compared to adults, and β3 integrin expression could only be detected in the choroid plexuses of rat pups (Fig.5D).

Importantly, similar results were obtained on human brain samples by immunohistochemistry analyses of the brain of a newborn (9 days old) and an adult (52 years old), for whom the causes of death were unrelated to meningitis. In the cortex, α5 integrin staining mainly revealed cerebral blood vessels in both neonate and adult. However, the staining intensity of the cerebral blood

vessels was strikingly more intense in the neonatal cortex compared to the adult. β3 expression in the neonate was very faint and observed in slightly bigger blood vessels than capillaries whereas it was totally absent in the adult cortex (Fig. 5E).

When brain sections from the ventricular area were specifically analyzed for α5 expression, a massive staining of all choroid plexuses blood vessels was observed in the neonatal specimen (Fig. 5F, arrows). In contrast and with the exception of few infiltrating cells, α5 expression was not detected in the adult specimen (Fig. 5F arrowheads). Similar to what was observed in the cortex, β3 expression was restricted to the biggest blood vessels in pups' choroid plexuses (Fig. 5F, arrows) and absent from smaller blood vessels (Fig. 5F, arrows heads) whereas it was totally absent in the adult choroid plexuses (Fig. 5F). Importantly, neither α5 nor β3 integrins were detected in choroid plexus epithelial cells of either the neonate or the adult (Fig. 5F). Altogether, these data indicate that α5β1 and αvβ3 integrins are overexpressed in human blood vessels of the BBB and the BCSFB during the neonatal period.

Initial brain penetration of CC17-GBS occurs at the BBB and BCSFB

CC17-GBS have been observed associated to both brain vessels of the BBB and choroid plexus of the BCSFB in a fatal case of neonatal LOD (15). However, the initial portal of entry of GBS in the brain remains unknown. To determine the initial entry site of CC17-GBS we used an *in vivo* murine bacteremia-derived meningitis model (6, 16). To carry out the experiments on a more amenable model than neonatal mice, we tested the presence of α5β1 and αvβ3 integrins in brain vessels of juvenile mice. These integrins were also still expressed at high level in juvenile compared to adult mice (Fig. 6A). Four hours after intravenous injection of juvenile mice with CC17-GFP strain, bacteria were found outside the blood vessels in the cortex and the choroid plexuses (Fig. 6B and C) indicating successful transmigration of CC17-GBS to the CNS at both the BBB and the BCSFB.

306 ***α5β1 and αvβ3 integrins are involved in the juvenile susceptibility to CC17-GBS meningitis***
307 **in vivo**
308 Next, we studied the relevance of the interaction between Srr2 adhesin and α5β1 and αvβ3
309 integrins *in vivo*. We first controlled the ability of BR_{Srr2} to recognize murine α5β1 and αvβ3
310 integrins validating the use of the murine model (Fig. S6). We compared the susceptibility to CC17-
311 GBS meningitis of juvenile mice to that of adult mice. In order to specifically address the
312 transmigration capacity to the CNS, we adapted the experiment to have the same bacteremia in
313 juvenile and adult mice. We found that infection with $2x10^7$ CFU in juvenile and $1.5x10^8$ CFU in
314 adult mice gave similar bacteremia at 4 h pi (Fig. 7A). Four hours after intravenous infection with
315 WT bacteria, significantly less bacteria were recovered from the brain of adult mice than of juvenile
316 mice demonstrating that juvenile mice are more susceptible to CC17 meningitis than adult mice
317 (Fig. 7B). We thus assayed the requirement for the Srr2 adhesin in meningitis development in
318 juvenile and adult mice and found that significantly less Δ*srr2* than WT bacteria were recovered
319 from the brain of juvenile mice (Fig. 7B). In contrast similar bacterial counts of the WT and the
320 Δ*srr2* mutant were recovered from adult brains (Fig. 7B). Furthermore, and whereas such was not
321 the case with juvenile mice, the brain of 33 % of adult mice infected with the WT strain was free
322 of bacteria, as in Δ*srr2*-infected juvenile and adult mice (38 and 27 % respectively). These results
323 demonstrate that Srr2 adhesin contributes to the early event of CC17-GBS transmigration to the
324 CNS in juvenile mice and does not contribute to the milder CNS transmigration in adult mice.
325 We therefore addressed the role of the integrins α5β1 and αvβ3 in the Srr2-dependent
326 susceptibility of juvenile mice. To establish the contribution of integrin α5β1, and since α5-integrin-
327 KO mice are embryonically lethal (40), we developed a model based on the use of blocking
328 antibody, a strategy successfully used for other meningeal pathogens (41). Anti-α5 integrin
329 neutralizing antibody or isotype control antibody-treated mice were infected intravenously with
330 CC17-GBS. The resulting bacteremia and total CFU counts 4 hours pi in the spleen and liver were

similar, but significantly reduced in the brain as compared with control condition (Fig. 7C). In contrast, anti-α5 integrin neutralizing antibody did not affect the capacity of the Δ*srr2* mutant to reach the brain as similar bacterial counts were recovered from brain of anti-α5 pretreated mice compared to control condition (Fig. 7D).

Similarly, as β3-integrin-KO mice suffer from vascular leakage (42), a blocking strategy was also used to investigate the αvβ3 integrin role in the early event of CC17-GBS transmigration to the CNS. Integrin αvβ3 was blocked using the mimetic peptide RGDfV which was highly efficient to inhibit BR_{Srr2}-αvβ3 interaction *in vitro* (Fig. 2C). RGDfV mimetic peptide or control vehicle-treated mice were infected with CC17-GBS. Administration of RGDfV mimetic peptide had no effect on bacteremia, spleen, and liver CFU counts 4 h pi, but decreased CC17-GBS penetration to the brain compared to the control vehicle (Fig. 7E), but not that of Δ*srr2* mutant (Fig. 7F).

Together, our data demonstrate that Srr2 interaction with α5β1 and αvβ3 integrins contributes to the juvenile mice susceptibility to CC17-GBS meningitis and that pre-treatments targeting these integrins reduce brain invasion.

DISCUSSION

Neonatal bacterial meningitis is a devastating life-threatening infection of the CNS. Despite antenatal screening of pregnant women associated with *intrapartum* antibiotic prophylaxis for GBS-positive mothers in most high-income countries, GBS remains the leading cause of neonatal meningitis. Meningitis cases due to GBS are accompanied with neurologic complications including seizure, hydrocephalus, subdural empyema, or cerebrovascular diseases and lead to 10% mortality and 25% permanent sequelae in surviving babies (43-45). Deciphering the mechanisms that drive the initial step of brain penetration by identifying the bacterial ligands and their cognate host cell receptors is of major clinical importance.

In our study, we demonstrate that the Srr2 adhesin, specifically and exclusively expressed by the hypervirulent CC17-GBS clone, mediates bacterial binding to brain endothelial cells by interacting

with the cellular host receptors integrins α5β1 and αvβ3. This interaction is essential for CC17-GBS to adhere and invade brain endothelial cells and contributes to meningitis development *in vivo*. Using a simplified cellular model, we demonstrate that α5β1 integrin is sufficient to promote CC17-GBS adhesion and internalization. In contrast, although recognized by Srr2 and being involved in adhesion and internalization into hCMEC/D3 and in meningitis development *in vivo*, αvβ3 integrin is not sufficient to trigger CC17-GBS adhesion and internalization in a cellular simplified model. This indicates that α5β1 integrin is *stricto sensu* a receptor for CC17-GBS, while αvβ3 integrin likely acts as a co-receptor as described for other pathogens (46). We also noticed that blocking the Srr2- integrin interaction of the WT CC17 strain, by competition with soluble integrins or by siRNA, did not reduce binding or invasion levels as much as deleting *srr2*. This could be explained either by the fact that blocking was not 100 % efficient or by the fact that Srr2 could recognize other receptors than α5β1 and αvβ3. Srr2 adhesin harbors two distinct binding motifs, RGD and SDV, which interact with the αvβ3 integrin. While numerous bacterial adhesins have been described to harbor an RGD motif, Srr2 is, to our knowledge, the first example of a bacterial adhesin harboring an SDV motif which is a newly described integrin binding motif (22). We have also shown, *via* an *in silico* approach confirmed by *in vitro* experiments, that Srr2 harbors two others motifs required for direct binding to the α5β1 integrin one in the N- and one in the C-terminal sub-domain of BR_{Srr2}. We have identified FSVKI as an important motif present on N-terminal domain of BR_{Srr2} for α5β1 integrin recognition. The pathophysiological relevance for the presence of two binding sites for each integrin is intriguing but has been described for other bacterial adhesins, *e.g.* from Group A *Streptococcus* that possesses several integrin binding sites on the same adhesin (47, 48). This probably reveals the importance of integrin recognition by those pathogens in the pathophysiology of the infection.

Our study highlights the role of integrins in the internalization process of CC17-GBS into endothelial cells. Although we did not investigate further the internalization mechanism, we found

that inhibitors of PI3K or Akt, that are molecules involved in integrins signaling, are not required for CC17-GBS internalization; rather, CC17-GBS internalization seems to be dependent on actin cytoskeleton, dynamin-2 and lipid rafts, as already described for other pathogens interacting with integrins (49).

How recognition of integrins by Srr2 adhesin enables bacterial entry into the brain is an important question that remains to be determined. On peripheral endothelial cells, bacterial adhesin-integrin interactions have been shown to promote bacterial vascular transmigration (50, 51). However, our current models of cerebral endothelial cells are not appropriate to investigate CC17-GBS transmigration mechanism. This could occur by transcellular and/or paracellular mechanism. Indeed, a transcellular crossing of the BBB has been described by Nizet *et al*. (14). But integrins are also known to be interconnected to cell junctions therefore being able to affect the vascular permeability in both peripheral and brain endothelial cell monolayers, which would lead to a paracellular transmigration for GBS (52-56). The latter has not been described upon GBS infection, yet some tight junction modifications upon GBS infection have been observed at later time points than 1 h (13, 57). Although speculative, direct Srr2-integrin interaction could therefore, in addition to CC17-GBS internalization in endothelial cells, lead to vascular permeability alteration favoring GBS paracellular transmigration at later time points. This hypothesis is reinforced by the fact that CC17-GBS strains strongly bind to fibrinogen in an Srr2-dependent manner (16, 17). $\alpha 5\beta 1$ and $\alpha v\beta 3$ integrins are host receptors for fibrinogen on endothelial cells. Fibrinogen fixation on its cellular receptors also leads to vascular permeability (58). Fibrinogen could therefore potentiate vascular permeability by acting as a bridging molecule between CC17-GBS and integrins, an indirect mechanism for integrin recognition largely employed by pathogens (59).

It has been previously shown that at the BBB, GBS exploits $\alpha 2\beta 1$ integrin in an indirect manner through collagen recognition (60). However, collagen recognition by GBS is not a conserved phenotype among GBS strains (61). This suggests that $\alpha 2\beta 1$ integrin recognition is likely not a

406 generalized mechanism to GBS strains. GBS also exploits α1β1 integrin in the vaginal tract (27,
407 62). However, α1β1 integrin is not expressed by brain endothelial cells (25) and we have shown
408 that neither Srr2 nor Srr1 bind α1β1 integrin (Fig. S3).
409 Previous studies had highlighted the presence of specific CC17 surface proteins and their role in
410 CC17 neurotropism (15-17, 63). By identifying α5β1 and αvβ3 as specific receptors for Srr2, we
411 provide new insights for the understanding of the neurotropism displayed by CC17 strains
412 compared to others GBS clones. The vast majority of GBS-elicited meningitis occurs during the
413 first three months of life (64) with the overwhelming majority of cases due to the CC17 clone (4,
414 9, 11). GBS can also cause meningitis or other invasive diseases in adults particularly among the
415 elderly, those with underlying diseases or had raw fish meal. However, in adults, the CC17 clone
416 is under-represented with most of the infections due to serotype V strains or strains belonging to
417 the ST283 sequence type, the recently identified clone linked to raw fish consumption (38, 65).
418 The reasons why CC17 is overrepresented in newborns compared to adults are largely unknown.
419 We have recently shown that perinatal hormones specifically favor CC17 pathogenesis by
420 promoting the maturation of intestinal M cells responsible for intestinal translocation (6). This
421 present work reveals that α5β1/αvβ3 integrins are overexpressed in neonatal blood vessels of the
422 BBB and BCSFB. The overexpression of α5β1/αvβ3 integrins detected during the neonatal period
423 could be due to the developmental switch of integrin expression occurring during the post-natal
424 period (66). This finding is of major clinical importance as the overexpression observed during the
425 post-natal period corresponds to the peak of CC17-elicited meningitis. Finally, no expression of
426 the α5β1/αvβ3 integrins was detected in choroid plexus epithelial cells. Yet, CC17 bacteria have
427 been observed closely associated to CPEC on brain slices of a fatal case of LOD (15), indicating
428 that CC17 must recognize other receptors than these two integrins to cross choroid plexus
429 epithelial cells.

The identification of specific host receptors favoring CC17-GBS brain penetration could represent useful targets for prevention and therapy of GBS meningitis. Indeed, our results show that pretreatments targeting these integrins can reduce brain invasion. Receptor blockade using antibodies or antagonists in adjunct treatment with antibiotics have high therapeutic potential. Several anti-integrin mAbs or integrin antagonists have been already developed and are currently used in various clinical or preclinical trials (67). The development of novel therapeutic strategies targeting the CC17-GBS is urgent, especially because LOD cases, for which the hypervirulent CC17-GBS is preponderant, have been continuously increasing over the last 20 years (10).

METHODS

Bacterial strains, plasmids, primers and antibodies

Bacterial strains, plasmids, primers and antibodies used in this study are listed in Table S1, S2, S3 and S4 respectively. *S. agalactiae* strains were cultured in Todd Hewitt (TH) in standing filled flasks broth or agar (Difco Laboratories, Detroit, MI) at 37°C. *Escherichia coli* was cultivated in Luria-Bertani (LB) medium. Antibiotics were used at the following concentrations: for *E. coli*, ampicillin 100 µg ml^{-1}; for *S. agalactiae,* spectinomycin 100 µg ml^{-1}.

Reagents

Recombinant human ICAM1 and human or mouse integrins (tested by the supplier for their ability to interact with known ligands) were from R&D system. The mimetic peptides RGDfV was from Sigma, RGDS and P11 were from Tocris. The Complete ™ Protease inhibitor cocktail was from Roche diagnostic and used following the manufacturer's instructions.

Expression and purification of His-tagged-BR recombinant peptides

Point mutations in putative integrin binding sites were inserted by site directed mutagenesis on pET2818-BR_{Srr2} (16) using the Quick-change XL II kit (Stratagen, Netherlands). After verification of the constructs by DNA sequencing, the constructed plasmids were introduced into *E. coli* BL21 for protein expression. Recombinant BR_{Srr2} regions were purified after induction with 1 mM of IPTG using Dynabeads (Life Technologies) following manufacturer instructions.

ELISA

To evaluate integrin or ICAM1 binding to immobilized BR_{Srr2} or BR_{Srr1} regions, ELISA assays were performed as follows: proteins were coated at 5 µg/mL overnight. After extensive wash and saturation with Bovine Serum Albumin (BSA-Probumin®, Millipore), 50 µL of ligand proteins (human integrins, ICAM1 or negative control BSA) were diluted at the specified concentrations in PBS containing 1% of BSA (Probumin®, Millipore) and incubated 2 h at 37°C. Integrin binding was assessed using antibodies listed in Table S4. Revelation was performed using OPD (Sigma) or TMB (Thermofisher). Values of the negative control obtained with BSA (Probumin®, Millipore)

were substracted to the signal. The effect of divalent cations on the interaction between BR_{Srr2} and integrins was tested by ELISA with the same protocol as above in the presence of 1 mM Mn^{2+} or 1 mM Ca^{2+}, as specified. Similarly, competition experiments were carried out by incubating 10 μg of integrins with immobilized BR_{Srr2} in the presence of increasing concentrations of mimetic peptides (RGDS, RGDfV or P11).

Bioinformatic analysis

In silico contact prediction of BR_{Srr2} (PDB code: 4MBR) interaction with α5β1 integrin (PDB code: 4WJK) was performed using the RaptorX Protein Complex Contact Prediction server (http://raptorx.uchicago.edu/ComplexContact/) (28). Graphic representation of predicted contacts between BR_{Srr2} and α5β1 integrin, identified by RaptorX, was generated using the PyMOL Molecular Graphics System, Version 2.0 Schrödinger, LLC.

Cell lines and culture conditions

Human brain microvascular endothelial cells (hCMEC/D3) were cultured as described previously (68). Chinese Ovary Hamster (CHO) stably transfected with human α5β1, αvβ3 or ICAM1 described and validated previously (30-32) were grown in DMEM containing non-essential amino acids and 5% Fetal Calf Serum (FCS) in the presence of appropriate antibiotic selection pressure. All cell lines were routinely tested for mycoplasma contamination (Mycoalert mycoplasma detection kit, LONZA).

siRNA transfection

To silence the expression of α5 or β3 integrin subunits, pools of four siRNA duplexes (ON-TARGET plus SMARTpool siRNA from Dharmacon) were used. The silencer select negative control-1 siRNA (Ambion) was used as negative control. hCMEC/D3 were transfected with siRNA using the Amaxa Nucleofactor Kit UVEC (Amaxa Biosystem) then seeded at 85 000 cells/cm^2 in twenty-four-well plates for 24 h. Transfected cells were transfected for a second time with 25 nM siRNA using Lipofectamine RNAiMAX Reagent (Invitrogen) according to the manufacturer's

instructions and incubated for a further 24 h. Cells were used 48 h after the first transfection. Efficiency of knockdown was assessed by Western Blot analysis.

Dot Blot and Western Blot analysis

For Dot Blot assay, 1 µg of human α5β1, αvβ3 and ICAM1 were dotted onto PVDF membranes placed in a Minifold Dot-Blot apparatus SRC-96/1 (Schleicher and Schuell). Strips were blocked with PBS containing 5% skim milk for 1 h. Interaction between immobilized α5β1, αvβ3 and ICAM1 (negative control) and BR_{Srr2} or BR_{Srr1} was realized by incubating strips overnight at 4°C in PBS containing 2% skim milk and 10 µg/ml of BR_{Srr1} or BR_{Srr2}. After incubation, the strips were washed 3 times in PBS Tween 0.05%, then incubated with anti-Srr2 or anti-Srr1 antibodies in 5% skim milk for 1 h at room temperature. Antisera raised against Srr1 and Srr2 are highly specific and display similar affinity (16).

For Western Blot, protein concentration was determined using the BCA protein assay kit (Thermoscientific). Proteins were separated by SDS-PAGE then transferred to PVDF membrane using the Trans-Blot Turbo transfer pack (Bio-Rad). Membranes were blocked in PBS containing 5% skimmed milk and incubated for 1 h with primary antibodies. Anti-actin directly coupled to HRP was used as a loading control for Western Blot.

After washing and incubation with HRP-conjugated secondary antibody (Jackson Immunoresearch West Grove, PA), strips from Dot Blot or membranes from Western Blot were revealed using the ECL detection system (Perkin-Elmer) and signals were detected using the chemiluminescence imaging system (Fusion, Vilber-Lourmat).

Association and invasion assays

Bacterial adhesion or invasion assays were performed in cellular culture media without FCS at a multiplicity of infection (MOI) of 10 bacteria per cell unless otherwise specified. Briefly, bacteria were grown to the mid-log phase, washed twice with sterile PBS then added to cells and centrifuged 5 min at 211g to synchronize infection. After 1 h of incubation at 37°C under a 5% CO_2 atmosphere, monolayers were washed 4 times with PBS. Cell-association was determined after

lysis with sterile H_2O. Appropriate dilutions were made in sterile PBS, then plated on TH agar and colony forming units (CFU) counted. The percent of association was calculated as follows: (CFU on plate count / CFU in inoculum) × 100. Assays were performed in triplicate and were repeated at least three times. When specified, results were expressed as normalized to the control condition.

For invasion assay 1 h-infected cell monolayers were treated for 30 min with cellular culture media containing penicillin/streptomycin (Gibco) and gentamicin (200 µg/ml) to kill extracellular bacteria. The monolayers were washed twice with PBS, and lysed with sterile H_2O. Appropriate dilutions were plated on TH agar and CFUs counted. The percent of invasion was calculated as follows: (CFU on plate count / CFU in inoculum) × 100. Assays were performed in triplicate and were repeated at least three times. When specified, results were expressed as normalized to the control condition. To decipher host signaling pathways during CC17-GBS internalization, hCMEC/D3 cells were pretreated with cytochalasin D (2µM), nocodazole (1µM), wortmannin (100nM), MK2206 (2µM), Methyl-β-cyclodextrin (2.5mM) or dynasore (80µM) for 1 h prior infection with CC17-GBS. Inhibitors were left during the time of infection at the same concentration except for dynasore for which concentration was dropped to 10µM. Treatments did not affect bacterial or cell viability (data not shown).

Immunofluorescent staining and image analysis

hCMEC/D3 cells were grown on Thermanox coverslips (Thermo Fischer Scientific). Isolated brain microvessels were sticked to slides using Cell Tak (Corning). Infected or non-infected cells or isolated brain microvessels were fixed in PBS containing 4% paraformaldehyde (PFA) for 10 min. Following fixation, samples were permeabilized by incubation in PBS containing 0.1% Triton-X100 for 4 min at room temperature then blocked for at least 1 h at room temperature in PBS containing 10% serum. Primary antibodies, diluted in 10% serum-PBS, were incubated for at least 1 h at room temperature. After 3 washes with PBS, samples were incubated for 1 h at room temperature with conjugated-secondary's antibodies (Jackson ImmunoResearch Laboratories) diluted in PBS

containing 10% serum. DAPI was used to counter-stain nuclei; phalloidin-633 or 594 to stain actin and isolectin B4-FITC to counter-stain microvessels. After 3 washes in PBS, coverslips were mounted in DAKO fluorescent mounting media (DAKO). Image acquisitions were realized using confocal laser scanning microscopy (Leica DMI6000) coupled to a spinning disk confocal head (YokogawaCSU-X1M1), controlled by the Metamorph 7.7.5 software. Images were processed using the ImageJ software.

To discriminate between extracellular and intracellular bacteria, cells were infected with GFP expressing bacteria. Extracellular GFP-expressing bacteria were counterstained in unpermeabilized conditions with an anti-GBS serum followed by a secondary rhodamine isothiocyanate-labeled antibody. Under these conditions, extracellular bacteria were green (GFP-labeled bacteria) and decorated with red (anti-GBS labeling), whereas intracellular bacteria were solely green (GFP-labeled bacteria).

Mechanical isolation of brain microvessels

Brain vessels from neonatal (2 days old), juvenile (3 weeks old) or adult (3 months old) rat or mice were isolated as described previously (69). Briefly, brains were collected, and triturated in a Potter-Thomas homogenizer. The homogenate was centrifuged and the pellet was resuspended in buffer containing 18% dextran. After centrifugation, myelin was eliminated and the pellet containing cerebral vessels was resuspended in a buffer containing 1% BSA. This suspension was filtered on a 20 µm Nylon Net filter and vessels fragments were recovered from the filter in a buffer containing 1% BSA. After final centrifugation, pellets of cerebral vessels were snap-frozen and kept at −80°C until used for Western Blot analysis or fixed to glass slides for immunofluorescence using Cell Tak (Corning).

Collection of lateral and 4th Ventricular Choroid Plexus

Choroid plexuses of both lateral and 4th ventricles dissected from neonatal (2-day-old) and adult rats under a stereomicroscope, as previously described, were provided by the Brain Interface

568 exploratory Platform (BIP, CRNL, Lyon, France) (70). The collected tissues were snap-frozen and
569 kept at −80°C until used.

570 **Immunohistochemistry**

571 Immunohistochemistry was performed by the Cochin HistIM Facility (Histology, Immunostaining,
572 laser, Microdissection). The paraffin embedded brain sections were cleared before incubation in
573 citrate buffer (pH 6.0). Expression of α5 or β3 integrin on sections was detected using the Bond
574 Polymer Refine Detection (Leica) kit with specific antibodies for α5 or β3 integrins and the
575 Immunostaining automaton (Bond III, Leica). Pictures were acquired using the slide scanner
576 (Lamina, Perkin Elmer).

577 **Animal experiments**

578 Juvenile (3 weeks old) and adult (3 months old) BALB/c mice were infected by intravenous
579 injection with $2x10^7$ and $1.5\ x10^8$ CFU respectively of exponentially growing GBS strains for 4 h.
580 For some experiments, juvenile mice were pretreated by injecting intravenously either 10 µg of
581 anti-α5 antibodies or isotype control, 5 mg/kg cyclic mimetic peptide RGDfV or PBS one hour
582 before challenge. No side effects in mice were observed following pre-treatment targeting $\alpha5\beta1$
583 or $\alpha v\beta3$ integrins. After 4 h of infection, mice were sacrificed, and, blood, spleen, liver and brain
584 were collected. The brain and spleen were homogenized in 1 mL of 0.9% sodium chloride using
585 a tissue homogenizer (Precellys system, Bertin Technologies) and liver were homogeneized in 9
586 mL using an Ultraturax. Serial dilutions in 0.9% sodium chloride were immediately plated on TH
587 agar for CFU counts. Bacterial counts in the brains were corrected for blood contamination using
588 the bacterial burden in the bloodstream and a conservative estimate of the mouse cerebral blood
589 volume of 2.5 ml per g tissue as described previously (71).
590 To study the portal of entry into the brain of CC17-GBS, juvenile mice were perfused and brains
591 were recovered and fixed overnight in PFA. The brains were embedded in 5% agarose and cut
592 into 500 µm-thick sections using a vibratome (Leica). The brain sections were clarified using Ethyl
593 cinnamate (Eci) (72) and immunostained using anti-CD31 (a marker for capillaries) and anti-

transthyretin (TTR, a marker for choroid plexuses) antibodies. The tissue sections were imaged using a Xplore Spinning confocal microscope. Images were processed using the ImageJ software.

Statistical analysis

All assays were performed at least in three independent experiments. Data represent mean ± SEM and statistical analyses were performed using GraphPad Prism 5.0 (GraphPad Software, San Diego, California). Significance levels were set at $*p \leq 0.05$; $**p \leq 0.01$;$***p \leq 0.001$.

Study approval

Written informed consent was obtained for all human samples used in this study.

All animal experiments described in this study were conducted in accordance with the guidelines of Paris Descartes University, in compliance with the European animal welfare regulation (http://ec.europa.eu/environment/chemicals/lab_animals/home_en.html) and were approved by the Institut Cochin University Paris Descartes animal care and use committee (CEEA34; Agreement number 2018021616168438).

AUTHOR CONTRIBUTIONS:

JG designed the research. RDDC, AP, ASB, CA, CC, AB, LC, and JG performed the experiments. GB performed *in silico* analysis of BR_{Srr2}-$\alpha5\beta1$ interaction. IP and CR provided anatomical pieces of human brain. ACB, MCS and JG performed brain microvessels purification. JG, RDDC, AP, AF analyzed the data. AF, AT, CP, EF and CAR provided intellectual input and guidance. JG wrote the manuscript and AF, AT, CP contributed to finalizing the manuscript. All authors discussed results and reviewed the final version of the manuscript.

ACKNOWLEDGMENTS

We are grateful to Pierre-Olivier Couraud (INSERM, Paris, France) for the gift of hCMEC/D3 cells, Alain Duperray for the gift of CHO-ICAM1 cells, Yoshikazu Takada for the gift of CHO-αvβ3 cells and Glen Ulett for the gift of the GFP plasmid. We are extremely grateful to Nathalie Strazielle and Jean-François Ghersi-Egea from Blood/brain Interfaces exploratory Platform (BIP, CRNL, Lyon,

France, https://crnl.univ-lyon1.fr/index.php/en/ Resource/Platforms/BIP) for choroid plexus isolation and helpful comments. We thank Matthieu Benard from the animal facility of the Institut Cochin and Marine Gaillard for their help with animal experiments and Thomas Guilbert and Fabienne Regnier for their help with brain slices clarification. We also thank the Imag'IC and HistIM core facilities of the Cochin Institute and Shaynoor Dramsi for anti-Srr1 antibody and for critical reading of the manuscript.

FINANCIAL SUPPORT

This work was supported by Agence Nationale de la Recherche (ANR) (Grant StrepB2brain, ANR-17-CE15-0026-01). LC is a recipient of a post-doctoral fellowship from the ANR (StrepB2brain). ASB is a doctoral fellow funded by Université de Paris. RDDC was funded by FERCM.

REFERENCES

1. Da Cunha, V., Davies, M.R., Douarre, P.E., Rosinski-Chupin, I., Margarit, I., Spinali, S., Perkins, T., Lechat, P., Dmytruk, N., Sauvage, E., et al. 2014. Streptococcus agalactiae clones infecting humans were selected and fixed through the extensive use of tetracycline. *Nat Commun* 5:4544.

2. Russell, N.J., Seale, A.C., O'Driscoll, M., O'Sullivan, C., Bianchi-Jassir, F., Gonzalez-Guarin, J., Lawn, J.E., Baker, C.J., Bartlett, L., Cutland, C., et al. 2017. Maternal Colonization With Group B Streptococcus and Serotype Distribution Worldwide: Systematic Review and Meta-analyses. *Clin Infect Dis* 65:S100-S111.

3. Edwards, M., Nizet, V., and Baker, C.J. 2011. CHAPTER 12 - Group B Streptococcal Infections. *Infectious Diseases of the Fetus and Newborn (Seventh Edition)* 419-469.

643 4. Joubrel, C., Tazi, A., Six, A., Dmytruk, N., Touak, G., Bidet, P., Raymond, J., Trieu Cuot,
644 P., Fouet, A., Kerneis, S., et al. 2015. Group B streptococcus neonatal invasive infections, France
645 2007-2012. *Clin Microbiol Infect* 21:910-916.
646 5. Morinis, J., Shah, J., Murthy, P., and Fulford, M. 2011. Horizontal transmission of group B
647 streptococcus in a neonatal intensive care unit. *Paediatr Child Health* 16:e48-50.
648 6. Hays, C., Touak, G., Bouaboud, A., Fouet, A., Guignot, J., Poyart, C., and Tazi, A. 2019.
649 Perinatal hormones favor CC17 group B Streptococcus intestinal translocation through M cells
650 and hypervirulence in neonates. *Elife* 8.
651 7. Tazi, A., Plainvert, C., Anselem, O., Ballon, M., Marcou, V., Seco, A., El Alaoui, F., Joubrel,
652 C., El Helali, N., Falloukh, E., et al. 2019. Risk Factors for Infant Colonization by Hypervirulent
653 CC17 Group B Streptococcus: Toward the Understanding of Late-onset Disease. *Clin Infect Dis*.
654 8. Lamy, M.C., Dramsi, S., Billoet, A., Reglier-Poupet, H., Tazi, A., Raymond, J., Guerin, F.,
655 Couve, E., Kunst, F., Glaser, P., et al. 2006. Rapid detection of the "highly virulent" group B
656 Streptococcus ST-17 clone. *Microbes Infect* 8:1714-1722.
657 9. Manning, S.D., Springman, A.C., Lehotzky, E., Lewis, M.A., Whittam, T.S., and Davies,
658 H.D. 2009. Multilocus sequence types associated with neonatal group B streptococcal sepsis and
659 meningitis in Canada. *J Clin Microbiol* 47:1143-1148.
660 10. Romain, A.S., Cohen, R., Plainvert, C., Joubrel, C., Bechet, S., Perret, A., Tazi, A., Poyart,
661 C., and Levy, C. 2018. Clinical and Laboratory Features of Group B Streptococcus Meningitis in
662 Infants and Newborns: Study of 848 Cases in France, 2001-2014. *Clin Infect Dis* 66:857-864.
663 11. Seale, A.C., Koech, A.C., Sheppard, A.E., Barsosio, H.C., Langat, J., Anyango, E.,
664 Mwakio, S., Mwarumba, S., Morpeth, S.C., Anampiu, K., et al. 2016. Maternal colonization with
665 Streptococcus agalactiae and associated stillbirth and neonatal disease in coastal Kenya. *Nat*
666 *Microbiol* 1:16067.
667 12. Coureuil, M., Lecuyer, H., Bourdoulous, S., and Nassif, X. 2017. A journey into the brain:
668 insight into how bacterial pathogens cross blood-brain barriers. *Nat Rev Microbiol* 15:149-159.

669 13. Kim, B.J., Hancock, B.M., Bermudez, A., Del Cid, N., Reyes, E., van Sorge, N.M., Lauth,
670 X., Smurthwaite, C.A., Hilton, B.J., Stotland, A., et al. 2015. Bacterial induction of Snail1
671 contributes to blood-brain barrier disruption. *J Clin Invest* 125:2473-2483.
672 14. Nizet, V., Kim, K.S., Stins, M., Jonas, M., Chi, E.Y., Nguyen, D., and Rubens, C.E. 1997.
673 Invasion of brain microvascular endothelial cells by group B streptococci. *Infect Immun* 65:5074-
674 5081.
675 15. Tazi, A., Disson, O., Bellais, S., Bouaboud, A., Dmytruk, N., Dramsi, S., Mistou, M.Y.,
676 Khun, H., Mechler, C., Tardieux, I., et al. 2010. The surface protein HvgA mediates group B
677 streptococcus hypervirulence and meningeal tropism in neonates. *J Exp Med* 207:2313-2322.
678 16. Six, A., Bellais, S., Bouaboud, A., Fouet, A., Gabriel, C., Tazi, A., Dramsi, S., Trieu-Cuot,
679 P., and Poyart, C. 2015. Srr2, a multifaceted adhesin expressed by ST-17 hypervirulent Group B
680 Streptococcus involved in binding to both fibrinogen and plasminogen. *Mol Microbiol* 97:1209-
681 1222.
682 17. Seo, H.S., Minasov, G., Seepersaud, R., Doran, K.S., Dubrovska, I., Shuvalova, L.,
683 Anderson, W.F., Iverson, T.M., and Sullam, P.M. 2013. Characterization of fibrinogen binding by
684 glycoproteins Srr1 and Srr2 of Streptococcus agalactiae. *J Biol Chem* 288:35982-35996.
685 18. Seo, H.S., Mu, R., Kim, B.J., Doran, K.S., and Sullam, P.M. 2012. Binding of glycoprotein
686 Srr1 of Streptococcus agalactiae to fibrinogen promotes attachment to brain endothelium and the
687 development of meningitis. *PLoS Pathog* 8:e1002947.
688 19. Wang, N.Y., Patras, K.A., Seo, H.S., Cavaco, C.K., Rosler, B., Neely, M.N., Sullam, P.M.,
689 and Doran, K.S. 2014. Group B streptococcal serine-rich repeat proteins promote interaction with
690 fibrinogen and vaginal colonization. *J Infect Dis* 210:982-991.
691 20. Bang, J.Y., Kim, E.Y., Kang, D.K., Chang, S.I., Han, M.H., Baek, K.H., and Kang, I.C. 2011.
692 Pharmacoproteomic analysis of a novel cell-permeable peptide inhibitor of tumor-induced
693 angiogenesis. *Mol Cell Proteomics* 10:M110 005264.

21. Ruoslahti, E. 1996. RGD and other recognition sequences for integrins. *Annu Rev Cell Dev Biol* 12:697-715.

22. Choi, Y., Kim, E., Lee, Y., Han, M.H., and Kang, I.C. 2010. Site-specific inhibition of integrin alpha v beta 3-vitronectin association by a ser-asp-val sequence through an Arg-Gly-Asp-binding site of the integrin. *Proteomics* 10:72-80.

23. Hynes, R.O., Lively, J.C., McCarty, J.H., Taverna, D., Francis, S.E., Hodivala-Dilke, K., and Xiao, Q. 2002. The diverse roles of integrins and their ligands in angiogenesis. *Cold Spring Harb Symp Quant Biol* 67:143-153.

24. Paulus, W., Baur, I., Schuppan, D., and Roggendorf, W. 1993. Characterization of integrin receptors in normal and neoplastic human brain. *Am J Pathol* 143:154-163.

25. Wang, J., and Milner, R. 2006. Fibronectin promotes brain capillary endothelial cell survival and proliferation through alpha5beta1 and alphavbeta3 integrins via MAP kinase signalling. *J Neurochem* 96:148-159.

26. Zhang, K., and Chen, J. 2012. The regulation of integrin function by divalent cations. *Cell Adh Migr* 6:20-29.

27. Bolduc, G.R., and Madoff, L.C. 2007. The group B streptococcal alpha C protein binds alpha1beta1-integrin through a novel KTD motif that promotes internalization of GBS within human epithelial cells. *Microbiology* 153:4039-4049.

28. Zeng, H., Wang, S., Zhou, T., Zhao, F., Li, X., Wu, Q., and Xu, J. 2018. ComplexContact: a web server for inter-protein contact prediction using deep learning. *Nucleic Acids Res* 46:W432-W437.

29. Schreiner, C.L., Bauer, J.S., Danilov, Y.N., Hussein, S., Sczekan, M.M., and Juliano, R.L. 1989. Isolation and characterization of Chinese hamster ovary cell variants deficient in the expression of fibronectin receptor. *J Cell Biol* 109:3157-3167.

718 30. Guignot, J., Hudault, S., Kansau, I., Chau, I., and Servin, A.L. 2009. Human decay-
719 accelerating factor and CEACAM receptor-mediated internalization and intracellular lifestyle of
720 Afa/Dr diffusely adhering Escherichia coli in epithelial cells. *Infect Immun* 77:517-531.
721 31. Takagi, J., Kamata, T., Meredith, J., Puzon-McLaughlin, W., and Takada, Y. 1997.
722 Changing ligand specificities of alphavbeta1 and alphavbeta3 integrins by swapping a short
723 diverse sequence of the beta subunit. *J Biol Chem* 272:19794-19800.
724 32. Sans, E., Delachanal, E., and Duperray, A. 2001. Analysis of the roles of ICAM-1 in
725 neutrophil transmigration using a reconstituted mammalian cell expression model: implication of
726 ICAM-1 cytoplasmic domain and Rho-dependent signaling pathway. *J Immunol* 166:544-551.
727 33. Bhattacharya, S., Ying, X., Fu, C., Patel, R., Kuebler, W., Greenberg, S., and
728 Bhattacharya, J. 2000. alpha(v)beta(3) integrin induces tyrosine phosphorylation-dependent
729 Ca(2+) influx in pulmonary endothelial cells. *Circ Res* 86:456-462.
730 34. Conforti, G., Dominguez-Jimenez, C., Zanetti, A., Gimbrone, M.A., Jr., Cremona, O.,
731 Marchisio, P.C., and Dejana, E. 1992. Human endothelial cells express integrin receptors on the
732 luminal aspect of their membrane. *Blood* 80:437-446.
733 35. Singh, B., Fu, C., and Bhattacharya, J. 2000. Vascular expression of the alpha(v)beta(3)-
734 integrin in lung and other organs. *Am J Physiol Lung Cell Mol Physiol* 278:L217-226.
735 36. Xanthis, I., Souilhol, C., Serbanovic-Canic, J., Roddie, H., Kalli, A.C., Fragiadaki, M.,
736 Wong, R., Shah, D.R., Askari, J.A., Canham, L., et al. 2019. beta1 integrin is a sensor of blood
737 flow direction. *J Cell Sci* 132.
738 37. van Kassel, M.N., Bijlsma, M.W., Brouwer, M.C., van der Ende, A., and van de Beek, D.
739 2019. Community-acquired group B streptococcal meningitis in adults: 33 cases from prospective
740 cohort studies. *J Infect* 78:54-57.
741 38. Luan, S.L., Granlund, M., Sellin, M., Lagergard, T., Spratt, B.G., and Norgren, M. 2005.
742 Multilocus sequence typing of Swedish invasive group B streptococcus isolates indicates a
743 neonatally associated genetic lineage and capsule switching. *J Clin Microbiol* 43:3727-3733.

744 39. Strazielle, N., and Ghersi-Egea, J.F. 2000. Choroid plexus in the central nervous system:
745 biology and physiopathology. *J Neuropathol Exp Neurol* 59:561-574.
746 40. Yang, J.T., Rayburn, H., and Hynes, R.O. 1993. Embryonic mesodermal defects in alpha
747 5 integrin-deficient mice. *Development* 119:1093-1105.
748 41. Iovino, F., Engelen-Lee, J.Y., Brouwer, M., van de Beek, D., van der Ende, A., Valls Seron,
749 M., Mellroth, P., Muschiol, S., Bergstrand, J., Widengren, J., et al. 2017. pIgR and PECAM-1 bind
750 to pneumococcal adhesins RrgA and PspC mediating bacterial brain invasion. *J Exp Med*
751 214:1619-1630.
752 42. Su, G., Atakilit, A., Li, J.T., Wu, N., Bhattacharya, M., Zhu, J., Shieh, J.E., Li, E., Chen, R.,
753 Sun, S., et al. 2012. Absence of integrin alphavbeta3 enhances vascular leak in mice by inhibiting
754 endothelial cortical actin formation. *Am J Respir Crit Care Med* 185:58-66.
755 43. Tibussek, D., Sinclair, A., Yau, I., Teatero, S., Fittipaldi, N., Richardson, S.E., Mayatepek,
756 E., Jahn, P., and Askalan, R. 2015. Late-onset group B streptococcal meningitis has
757 cerebrovascular complications. *J Pediatr* 166:1187-1192 e1181.
758 44. Kohli-Lynch, M., Russell, N.J., Seale, A.C., Dangor, Z., Tann, C.J., Baker, C.J., Bartlett,
759 L., Cutland, C., Gravett, M.G., Heath, P.T., et al. 2017. Neurodevelopmental Impairment in
760 Children After Group B Streptococcal Disease Worldwide: Systematic Review and Meta-analyses.
761 *Clin Infect Dis* 65:S190-S199.
762 45. Andrade, E.B., Magalhaes, A., Puga, A., Costa, M., Bravo, J., Portugal, C.C., Ribeiro, A.,
763 Correia-Neves, M., Faustino, A., Firon, A., et al. 2018. A mouse model reproducing the
764 pathophysiology of neonatal group B streptococcal infection. *Nat Commun* 9:3138.
765 46. Wang, X., Huang, D.Y., Huong, S.M., and Huang, E.S. 2005. Integrin alphavbeta3 is a
766 coreceptor for human cytomegalovirus. *Nat Med* 11:515-521.
767 47. Humtsoe, J.O., Kim, J.K., Xu, Y., Keene, D.R., Hook, M., Lukomski, S., and Wary, K.K.
768 2005. A streptococcal collagen-like protein interacts with the alpha2beta1 integrin and induces
769 intracellular signaling. *J Biol Chem* 280:13848-13857.

48. Weckel, A., Ahamada, D., Bellais, S., Mehats, C., Plainvert, C., Longo, M., Poyart, C., and Fouet, A. 2018. The N-terminal domain of the R28 protein promotes emm28 group A Streptococcus adhesion to host cells via direct binding to three integrins. *J Biol Chem* 293:16006-16018.

49. Gianni, T., Gatta, V., and Campadelli-Fiume, G. 2010. {alpha}V{beta}3-integrin routes herpes simplex virus to an entry pathway dependent on cholesterol-rich lipid rafts and dynamin2. *Proc Natl Acad Sci U S A* 107:22260-22265.

50. Kumar, D., Ristow, L.C., Shi, M., Mukherjee, P., Caine, J.A., Lee, W.Y., Kubes, P., Coburn, J., and Chaconas, G. 2015. Intravital Imaging of Vascular Transmigration by the Lyme Spirochete: Requirement for the Integrin Binding Residues of the B. burgdorferi P66 Protein. *PLoS Pathog* 11:e1005333.

51. Ristow, L.C., Bonde, M., Lin, Y.P., Sato, H., Curtis, M., Wesley, E., Hahn, B.L., Fang, J., Wilcox, D.A., Leong, J.M., et al. 2015. Integrin binding by Borrelia burgdorferi P66 facilitates dissemination but is not required for infectivity. *Cell Microbiol* 17:1021-1036.

52. Alghisi, G.C., Ponsonnet, L., and Ruegg, C. 2009. The integrin antagonist cilengitide activates alphaVbeta3, disrupts VE-cadherin localization at cell junctions and enhances permeability in endothelial cells. *PLoS One* 4:e4449.

53. Engelhardt, B. 2011. beta1-integrin/matrix interactions support blood-brain barrier integrity. *J Cereb Blood Flow Metab* 31:1969-1971.

54. Hermann, D.M., and ElAli, A. 2012. The abluminal endothelial membrane in neurovascular remodeling in health and disease. *Sci Signal* 5:re4.

55. Osada, T., Gu, Y.H., Kanazawa, M., Tsubota, Y., Hawkins, B.T., Spatz, M., Milner, R., and del Zoppo, G.J. 2011. Interendothelial claudin-5 expression depends on cerebral endothelial cell-matrix adhesion by beta(1)-integrins. *J Cereb Blood Flow Metab* 31:1972-1985.

56. Pulous, F.E., and Petrich, B.G. 2019. Integrin-dependent regulation of the endothelial barrier. *Tissue Barriers* 7:1685844.

796 57. Kim, B.J., Bee, O.B., McDonagh, M.A., Stebbins, M.J., Palecek, S.P., Doran, K.S., and
797 Shusta, E.V. 2017. Modeling Group B Streptococcus and Blood-Brain Barrier Interaction by Using
798 Induced Pluripotent Stem Cell-Derived Brain Endothelial Cells. *mSphere* 2.
799 58. Davalos, D., and Akassoglou, K. 2012. Fibrinogen as a key regulator of inflammation in
800 disease. *Semin Immunopathol* 34:43-62.
801 59. Hauck, C.R., Borisova, M., and Muenzner, P. 2012. Exploitation of integrin function by
802 pathogenic microbes. *Curr Opin Cell Biol* 24:637-644.
803 60. Banerjee, A., Kim, B.J., Carmona, E.M., Cutting, A.S., Gurney, M.A., Carlos, C., Feuer, R.,
804 Prasadarao, N.V., and Doran, K.S. 2011. Bacterial Pili exploit integrin machinery to promote
805 immune activation and efficient blood-brain barrier penetration. *Nat Commun* 2:462.
806 61. Dramsi, S., Morello, E., Poyart, C., and Trieu-Cuot, P. 2012. Epidemiologically and
807 clinically relevant Group B Streptococcus isolates do not bind collagen but display enhanced
808 binding to human fibrinogen. *Microbes Infect* 14:1044-1048.
809 62. Vornhagen, J., Armistead, B., Santana-Ufret, V., Gendrin, C., Merillat, S., Coleman, M.,
810 Quach, P., Boldenow, E., Alishetti, V., Leonhard-Melief, C., et al. 2018. Group B streptococcus
811 exploits vaginal epithelial exfoliation for ascending infection. *J Clin Invest* 128:1985-1999.
812 63. Brochet, M., Couve, E., Zouine, M., Vallaeys, T., Rusniok, C., Lamy, M.C., Buchrieser, C.,
813 Trieu-Cuot, P., Kunst, F., Poyart, C., et al. 2006. Genomic diversity and evolution within the
814 species Streptococcus agalactiae. *Microbes Infect* 8:1227-1243.
815 64. Phares, C.R., Lynfield, R., Farley, M.M., Mohle-Boetani, J., Harrison, L.H., Petit, S., Craig,
816 A.S., Schaffner, W., Zansky, S.M., Gershman, K., et al. 2008. Epidemiology of invasive group B
817 streptococcal disease in the United States, 1999-2005. *JAMA* 299:2056-2065.
818 65. Kalimuddin, S., Chen, S.L., Lim, C.T.K., Koh, T.H., Tan, T.Y., Kam, M., Wong, C.W.,
819 Mehershahi, K.S., Chau, M.L., Ng, L.C., et al. 2017. 2015 Epidemic of Severe Streptococcus
820 agalactiae Sequence Type 283 Infections in Singapore Associated With the Consumption of Raw

Freshwater Fish: A Detailed Analysis of Clinical, Epidemiological, and Bacterial Sequencing Data. *Clin Infect Dis* 64:S145-S152.

66. Milner, R., and Campbell, I.L. 2002. Developmental regulation of beta1 integrins during angiogenesis in the central nervous system. *Mol Cell Neurosci* 20:616-626.

67. Raab-Westphal, S., Marshall, J.F., and Goodman, S.L. 2017. Integrins as Therapeutic Targets: Successes and Cancers. *Cancers (Basel)* 9.

68. Weksler, B., Romero, I.A., and Couraud, P.O. 2013. The hCMEC/D3 cell line as a model of the human blood brain barrier. *Fluids Barriers CNS* 10:16.

69. Boulay, A.C., Saubamea, B., Decleves, X., and Cohen-Salmon, M. 2015. Purification of Mouse Brain Vessels. *J Vis Exp*:e53208.

70. Kratzer, I., Liddelow, S.A., Saunders, N.R., Dziegielewska, K.M., Strazielle, N., and Ghersi-Egea, J.F. 2013. Developmental changes in the transcriptome of the rat choroid plexus in relation to neuroprotection. *Fluids Barriers CNS* 10:25.

71. Doran, K.S., Liu, G.Y., and Nizet, V. 2003. Group B streptococcal beta-hemolysin/cytolysin activates neutrophil signaling pathways in brain endothelium and contributes to development of meningitis. *J Clin Invest* 112:736-744.

72. Vigouroux, R.J, Belle, M., and Chédotal, A. 2017. Neuroscience in the third dimension: shedding new light on the brain with tissue clearing. Mol. Brain 10:33

FIGURE LEGENDS

Figure 1: BR_{Srr2} recognizes α5β1 and αvβ3 integrins in a direct manner. (A) Schematic representation of Srr2 and Srr1 proteins with signal sequence (checkered), serine-rich regions (white), LPxTG cell wall anchoring motif (hatched) and the binding regions of Srr2 (black) or Srr1 (grey) delineated by dashed lines. Numbers in black indicate the position of amino acid residues and letters in white indicate the predicted motifs of interaction with integrins. (B) Dot Blotting was performed to determine the interaction between immobilized human α5β1, αvβ3 integrins or ICAM1 and BR_{Srr2} or BR_{Srr1}. Purified BR_{Srr2} and BR_{Srr1} proteins are shown in Fig. S1A. (C, D and E) Interaction of BR_{Srr2} (black squares) or BR_{Srr1} (grey circles) with human α5β1 integrin (C), αvβ3 integrin (D) or ICAM1 (E) were assessed by ELISA. Results were normalized to negative control (BSA). Statistical analysis: data shown are mean ± SEM of at least three independent experiments. Two-Way ANOVA with Bonferroni's multiple comparisons post-test was performed. NS, non-significant; *, $p < 0.05$; **, $p < 0.01$; ***, $p < 0.001$.

Figure 2: Identification of BR_{Srr2} residues involved in the direct interaction with αvβ3 and α5β1 integrins. (A and B) Interaction of BR_{Srr2}, or its mutated forms, with integrins αvβ3 (A) or α5β1 (B) were assessed by ELISA. Mutated forms of BR_{Srr2} proteins are shown in Supplementary Fig. S1B and C. (C and D) Interaction of BR_{Srr2} with integrins αvβ3 (C) or α5β1 (D) in the presence of increasing concentration of mimetic peptides were assessed by ELISA. Results were expressed as % of untreated condition. (E) Graphic representation of predicted contacts between BR_{Srr2} and α5β1 integrin identified by RaptorX (Fig. S4). RaptorX mapped on the α5 (grey) β1 (green) integrin subunits predicted two contact zones located in the N-terminal (blue) and C-terminal (gold) domains of BR_{Srr2}. Only the most reliable contacts (contact probability >0.7) are depicted as yellow lines in the scheme. (F) Schematic representation of BR_{Srr2} or its truncated forms. Numbers in black indicate the position of amino acid residues in Srr2, and letters in white the predicted motifs of interaction with the integrin α5β1. (G) ELISA assays with integrin α5β1 were performed using equimolar amounts of coated BR_{Srr2} or of its truncated forms. (H) Interaction of BR_{Srr2}, or its

mutated forms, with the integrin α5β1 were assessed by ELISA. Mutated forms of BR_{Srr2} proteins are shown in Fig. S1D and E.

ELISA results were normalized to the negative control (BSA). Statistical analysis: data shown are mean ± SEM of at least three independent experiments. Two-Way ANOVA with Bonferroni's multiple comparisons post-test was performed. NS, non-significant; *, $p < 0.05$; **, $p < 0.01$; ***, $p < 0.001$.

Figure 3: α5β1 promotes adhesion and invasion of CC17-GBS in a simplified model of CHO cells. (A and B) CHO, CHO-α5β1, CHO-αvβ3, CHO-ICAM1 were infected with GBS strains for 1 h then subjected to (A, B and E) immunofluorescence analysis or (C, D and F) CFU counts. (A) Representative micrographs of untransfected or transfected CHO cells infected with CC17-GFP (green). Nuclei were labeled with DAPI (blue) and actin with phalloidin (grey). Scale bar: 10 µm. (B) Representative micrographs of transfected CHO-α5β1 infected with CC17-GFP strain (green) and immunostained with anti α5-integrin antibody (red). Two independent fields from the same experiment are shown. Scale bar: 10 µm. (C) Adhesion of a CC17 or a non-CC17 (CC23) strain on transfected or untransfected CHO cells was quantified. Results are expressed as the % of adhesion obtained on transfected cells minus that obtained on untransfected cells. (D) Adhesion level of WT CC17 and derived strains on CHO-α5β1 normalized to WT CC17 adhesion. Anti-Srr2 antibody was diluted 1/500. (E) CC17-GFP strain (green) was used to infect CHO-α5β1. Differential staining was realized to discriminate extracellular from intracellular bacteria. GBS outside of host cells have green (GFP) and red fluorescence (anti-GBS) and appear yellow/red, whereas bacteria inside host cells have green fluorescence only. Nuclei were labeled with DAPI (blue) and actin was stained using phalloidin (grey). Scale bar: 10 µm. Boxed area corresponds to magnification of inset. (F) Invasion of CC17 strain or Δ*srr2*-derived strain on untransfected CHO or CHO-α5β1 was quantified by CFU counts. All experiments were performed at least three times with each condition.

892 Statistical analysis: Data shown are mean ± SEM of at least 3 independent experiments realized
893 in triplicate. One-Way ANOVA with Tukey's (C, F), Dunn's (D) multiple comparison test were
894 performed. NS, non-significant; *, $p < 0.05$; **, $p < 0.01$; *** p<0.001.

895 **Figure 4: α5β1 and αvβ3 integrins promote Srr2 dependent CC17-GBS attachment and**
896 **invasion of cerebral endothelial cells.** (A, B) Adhesion of GBS strains onto hCMEC/D3 was
897 assessed by CFU counts (A) at MOI 10 (B) at MOI 1 in the absence or the presence of 10 µg/ml
898 of recombinant human soluble α5β1 (s-α5β1 integrin) or αvβ3 (s-αvβ3 integrin) or a mix of both
899 integrins (s-α5β1 + s-αvβ3 integrins), or ICAM1 (s-ICAM1). For each strain, results were
900 normalized to those obtained in the control experiment (untreated). (C, D) Depletion of relevant
901 integrin subunit in siRNA knockdown of (C) α5 integrin (D) β3 integrin in hCMEC/D3 were analyzed
902 by Western Blot. (E) Adhesion of GBS strains onto cerebral endothelial cells, control (si-scramble),
903 α5 integrin-depleted (si-α5 integrin), β3 integrin-depleted (si-β3 integrin), α5 and β3 integrin-
904 depleted (si-α5 + si-β3 integrins), quantified by CFU following a 1 h infection. For each strain,
905 results were normalized to those obtained in the control experiment (si-scramble). (F) CC17-GFP
906 strain (green) was used to infect cerebral endothelial cells. Differential staining allowing to
907 discriminate intracellular (green) from extracellular (green + red) bacteria was performed as in Fig.
908 3E. Nuclei: DAPI (blue) and ZO1 (grey)**.** Scale bar: 5 µm. (G) Invasion of GBS strains in
909 hCMEC/D3 was quantified by CFU counts. (H) Invasion of GBS strains in hCMEC/D3. For each
910 strain, results were normalized to those obtained in the control experiment (si-scramble). (H)
911 Invasion of CC17 strain in hCMEC/D3 was realized in the presence of host cell signaling inhibitors
912 and normalized to untreated condition.
913 Statistical analysis: Experiments were performed at least three times with each condition in
914 triplicate and expressed as mean ± SEM. One-Way ANOVA with Dunn's multiple comparison test
915 were performed. NS, non-significant; * $p < 0.05$; **, $p < 0.01$, ****, $p < 0.0001$.

916 **Figure 5: α5β1 and αvβ3 integrins are overexpressed during the post-natal period.**
917 Expression of α5β1 or αvβ3 integrins in neonates (Neo.) or adults (Ad.) were analyzed by (A and

C) immunofluorescence (N=2), (B and D) Western Blot (N=3) or (E and F) immunohistochemistry (N=2). (A and B) Purified rat brain vessels (BV) were labeled with specific antibodies to (A) α5 integrin to visualize α5β1 expression or (B) β3 integrin to visualize αvβ3 expression. BV were counter-stained using FITC-isolectin B4 and nuclei were labeled with DAPI. Scale bar: 20 µm. Similar contrast adjustment was applied between neonates and adults images. (C and D) 100 µg of rat (C) BV or (D) choroid plexus from 4th ventricle (CP4V) or lateral ventricles (CPLV) were subjected to Western Blot analysis. Actin was used as loading control. (E and F) Sections of human brain tissue were subjected to immunohistochemistry using antibodies to α5 or β3 integrins to visualize α5β1 or αvβ3 respectively, then counterstained with hematoxylin. Representative micrographs of cortex allowing to visualize (E) BV, scale bar: 100 µm or (F) choroid plexuses, scale bar: 50 µm. Arrows indicate BV from choroid vessels displaying positive staining; arrow-heads indicate BV displaying negative staining. Boxed areas correspond to magnification of insets.

Figure 6: Initial brain penetration of CC17-GBS occurs *via* blood vessels from the cortex and the choroid plexuses. Expression of α5β1 or αvβ3 integrins on purified brain vessels (BV) from neonatal (Neo.), juvenile (Juv.) or adult (Ad.) Balb/C mice was analyzed by Western Blot (N=2) (A) Juvenile mice were infected for 4 h with CC17-GFP strain (green) (N=2). Cerebral blood vessels were stained with CD31 (red) and choroid plexus with anti-TTR (cyan). Cortex (B) and choroid plexuses from the lateral ventricles (C) were examined. CC17-GFP bacteria were found associated with blood vessels (arrowheads) and at distance from blood vessels (arrows). Scale bar = 5 µm.

Figure 7: α5β1 and αvβ3 integrins contribute to the juvenile-specific CC17-GBS-elicited meningitis *in vivo*.

Juvenile or adult Balb/C mice were infected by intravenous injection with WT CC17 (white circles) or Δ*srr2* mutant (black squares) for 4h. Mice were euthanized and bacterial loads in blood (CFU/ml) (A) and brain (CFU/g) (B) were quantified. Each symbol represents the numeration from

one organ from one mouse. Red horizontal lines indicate medians. Statistical analysis: Two-Way ANOVA with Bonferroni's post-test was performed. NS, non-significant; * $p < 0.05$; **, $p < 0.01$. Juvenile Balb/C mice were pre-treated by (C and D) intravenous injection of 10 µg of anti-α5 antibody to block α5β1 integrin or 10 µg of isotype control, or (E and F) 5 mg/kg of RGDfV mimetic peptide to block αvβ3 or control vehicle (PBS). One hour after pre-treatment, mice were infected by intravenous injection with $2x10^7$ CFU of WT CC17 (C and E) or Δ*srr2* mutant (D and F) for 4 h. Mice were euthanized and bacterial loads in blood (CFU/ml), spleen, liver, and brain (CFU/g) were quantified. Each symbol represents the numeration from one organ from one mouse. White circles: control mice; black squares: treated mice. Red horizontal lines indicate medians. Statistical analysis: Mann-Whitney t test were performed with, NS, non-significant; *, $p < 0.05$; **, $p < 0.01$.

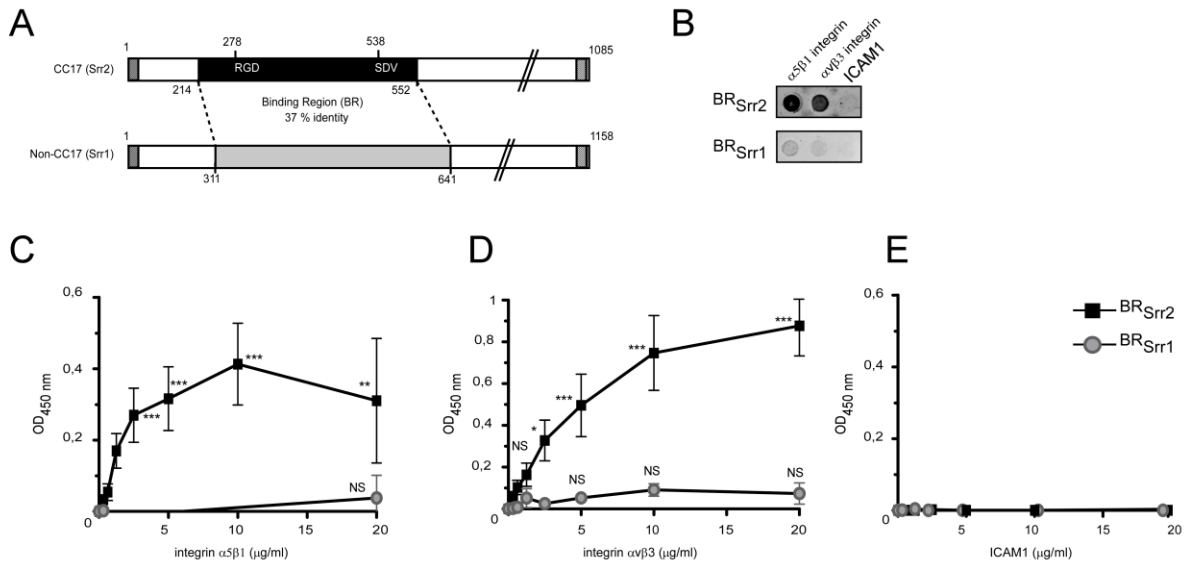

954

955 **Figure 1: BR_{Srr2} recognizes α5β1 and αvβ3 integrins in a direct manner.** (A) Schematic
956 representation of Srr2 and Srr1 proteins with signal sequence (checkered), serine-rich regions
957 (white), LPxTG cell wall anchoring motif (hatched) and the binding regions of Srr2 (black) or Srr1
958 (grey) delineated by dashed lines. Numbers in black indicate the position of amino acid residues
959 and letters in white indicate the predicted motifs of interaction with integrins. (B) Dot Blotting was
960 performed to determine the interaction between immobilized human α5β1, αvβ3 integrins or
961 ICAM1 and BR_{Srr2} or BR_{Srr1}. Purified BR_{Srr2} and BR_{Srr1} proteins are shown in Fig. S1A. (C, D and
962 E) Interaction of BR_{Srr2} (black squares) or BR_{Srr1} (grey circles) with human α5β1 integrin (C), αvβ3
963 integrin (D) or ICAM1 (E) were assessed by ELISA. Results were normalized to negative control
964 (BSA). Statistical analysis: data shown are mean ± SEM of at least three independent
965 experiments. Two-Way ANOVA with Bonferroni's multiple comparisons post-test was performed.
966 NS, non-significant; *, $p < 0.05$; **, $p < 0.01$; ***, $p < 0.001$.

967

968

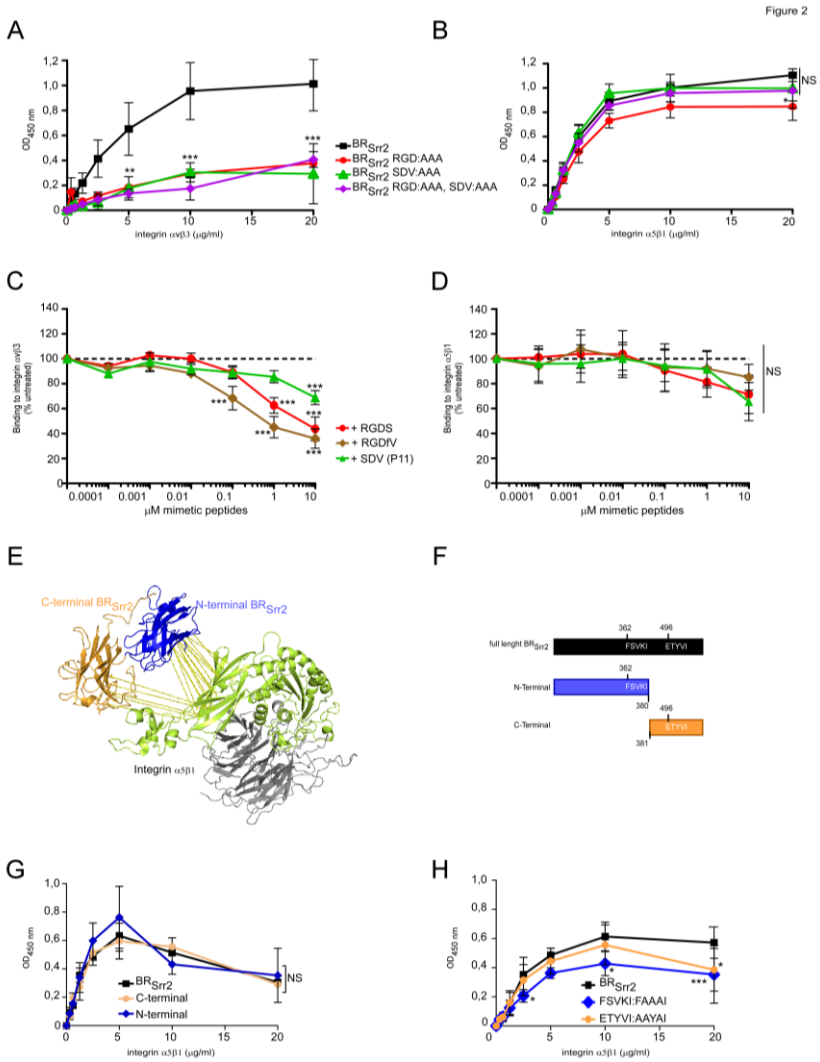

Figure 2: Identification of BR_{Srr2} residues involved in the direct interaction with αvβ3 and α5β1 integrins. (A and B) Interaction of BR_{Srr2}, or its mutated forms, with integrins αvβ3 (A) or α5β1 (B) were assessed by ELISA. Mutated forms of BR_{Srr2} proteins are shown in Supplementary Fig. S1B and C. (C and D) Interaction of BR_{Srr2} with integrins αvβ3 (C) or α5β1 (D) in the presence of increasing concentration of mimetic peptides were assessed by ELISA. Results were expressed as % of untreated condition. (E) Graphic representation of predicted contacts between BR_{Srr2} and α5β1 integrin identified by RaptorX (Fig. S4). RaptorX mapped on the α5 (grey) β1 (green) integrin subunits predicted two contact zones located in the N-terminal (blue) and C-terminal (gold) domains of BR_{Srr2}. Only the most reliable contacts (contact probability >0.7) are depicted as yellow lines in the scheme. (F) Schematic representation of BR_{Srr2} or its truncated forms. Numbers in black indicate the position of amino acid residues in Srr2, and letters in white the predicted motifs of interaction with the integrin α5β1. (G) ELISA assays with integrin α5β1 were performed using equimolar amounts of coated BR_{Srr2} or of its truncated forms. (H) Interaction of BR_{Srr2}, or its mutated forms, with the integrin α5β1 were assessed by ELISA. Mutated forms of BR_{Srr2} proteins are shown in Fig. S1D and E.

ELISA results were normalized to the negative control (BSA). Statistical analysis: data shown are mean ± SEM of at least three independent experiments. Two-Way ANOVA with Bonferroni's multiple comparisons post-test was performed. NS, non-significant; *, $p < 0.05$; **, $p < 0.01$; ***, $p < 0.001$.

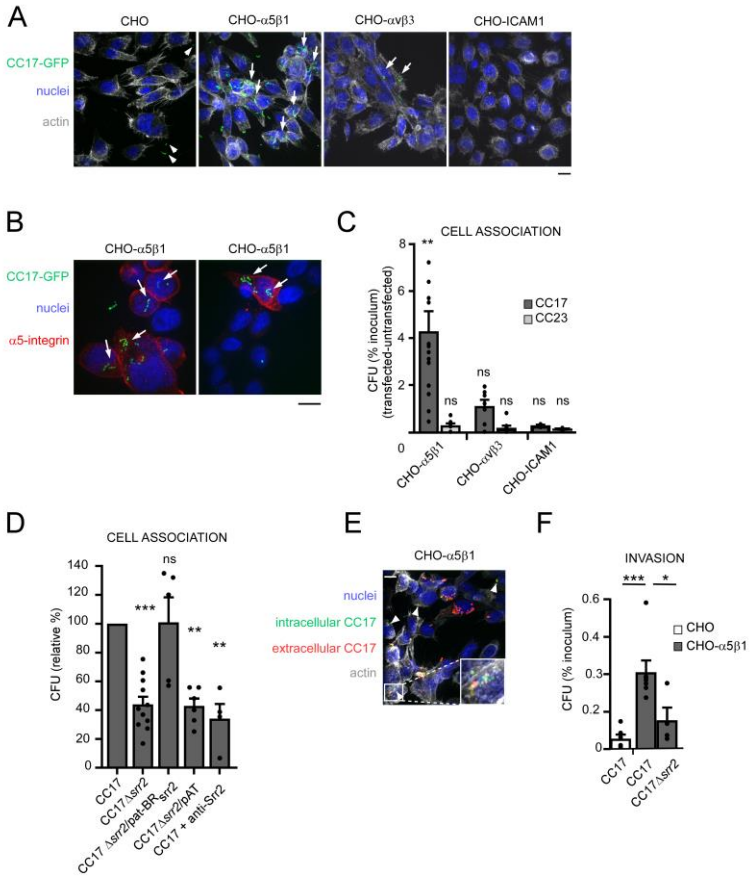

Figure 3: α5β1 promotes adhesion and invasion of CC17-GBS in a simplified model of CHO cells. (A and B) CHO, CHO-α5β1, CHO-αvβ3, CHO-ICAM1 were infected with GBS strains for 1 h then subjected to (A, B and E) immunofluorescence analysis or (C, D and F) CFU counts. (A) Representative micrographs of untransfected or transfected CHO cells infected with CC17-GFP (green). Nuclei were labeled with DAPI (blue) and actin with phalloidin (grey). Scale bar: 10 µm. (B) Representative micrographs of transfected CHO-α5β1 infected with CC17-GFP strain (green) and immunostained with anti α5-integrin antibody (red). Two independent fields from the same experiment are shown. Scale bar: 10 µm. (C) Adhesion of a CC17 or a non-CC17 (CC23) strain on transfected or untransfected CHO cells was quantified. Results are expressed as the % of adhesion obtained on transfected cells minus that obtained on untransfected cells. (D) Adhesion level of WT CC17 and derived strains on CHO-α5β1 normalized to WT CC17 adhesion. Anti-Srr2 antibody was diluted 1/500. (E) CC17-GFP strain (green) was used to infect CHO-α5β1. Differential staining was realized to discriminate extracellular from intracellular bacteria. GBS outside of host cells have green (GFP) and red fluorescence (anti-GBS) and appear yellow/red, whereas bacteria inside host cells have green fluorescence only. Nuclei were labeled with DAPI (blue) and actin was stained using phalloidin (grey). Scale bar: 10 µm. Boxed area corresponds to magnification of inset. (F) Invasion of CC17 strain or Δ*srr2*-derived strain on untransfected CHO or CHO-α5β1 was quantified by CFU counts.

Statistical analysis: Data shown are mean ± SEM of at least 3 independent experiments realized in triplicate. One-Way ANOVA with Tukey's (C, F), Dunn's (D) multiple comparison test were performed. NS, non-significant; *, $p < 0.05$; **, $p < 0.01$; *** p<0.001. All experiments were performed at least three times with each condition.

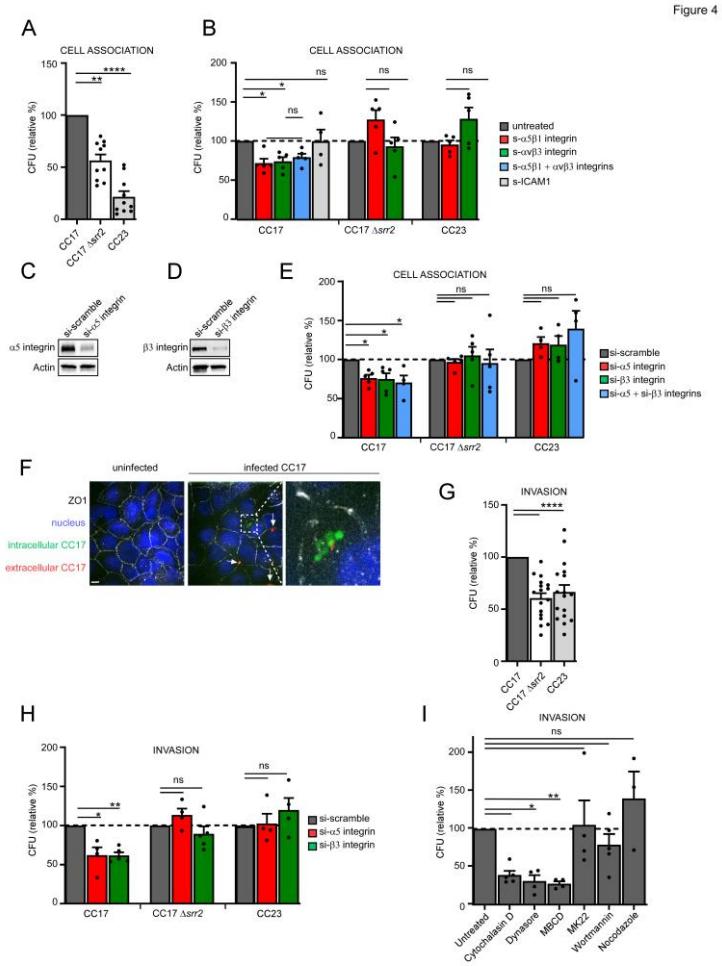

Figure 4: α5β1 and αvβ3 integrins promote Srr2 dependent CC17-GBS attachment and invasion of cerebral endothelial cells. (A, B) Adhesion of GBS strains onto hCMEC/D3 was assessed by CFU counts (A) at MOI 10 (B) at MOI 1 in the absence or the presence of 10 µg/ml of recombinant human soluble α5β1 (s-α5β1 integrin) or αvβ3 (s-αvβ3 integrin) or a mix of both integrins (s-α5β1 + s-αvβ3 integrins), or ICAM1 (s-ICAM1). For each strain, results were normalized to those obtained in the control experiment (untreated). (C, D) Depletion of relevant integrin subunit in siRNA knockdown of (C) α5 integrin (D) β3 integrin in hCMEC/D3 were analyzed by Western Blot. (E) Adhesion of GBS strains onto cerebral endothelial cells, control (si-scramble), α5 integrin-depleted (si-α5 integrin), β3 integrin-depleted (si-β3 integrin), α5 and β3 integrin-depleted (si-α5 + si-β3 integrins), quantified by CFU following a 1 h infection. For each strain, results were normalized to those obtained in the control experiment (si-scramble). (F) CC17-GFP strain (green) was used to infect cerebral endothelial cells. Differential staining allowing to discriminate intracellular (green) from extracellular (green + red) bacteria was performed as in Fig. 3E. Nuclei: DAPI (blue) and ZO1 (grey)**.** Scale bar: 5 µm. (G) Invasion of GBS strains in hCMEC/D3 was quantified by CFU counts. (H) Invasion of GBS strains in hCMEC/D3. For each strain, results were normalized to those obtained in the control experiment (si-scramble). (H) Invasion of CC17 strain in hCMEC/D3 was realized in the presence of host cell signaling inhibitors and normalized to untreated condition.

Statistical analysis: Experiments were performed at least three times with each condition in triplicate and expressed as mean ± SEM. One-Way ANOVA with Dunn's multiple comparison test were performed. NS, non-significant; * $p < 0.05$; **, $p < 0.01$, ****, $p < 0.0001$.

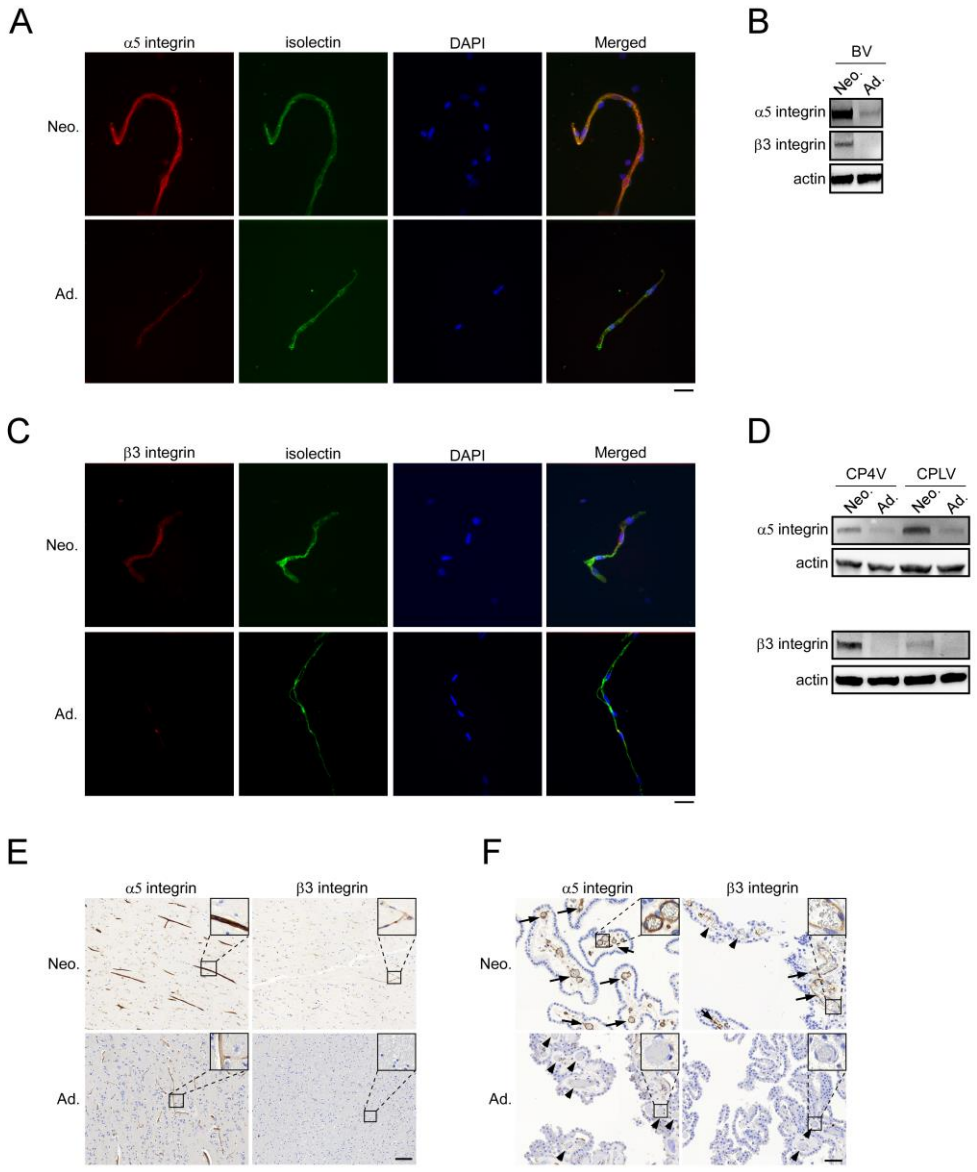

Figure 5: α5β1 and αvβ3 integrins are overexpressed during the post-natal period. Expression of α5β1 or αvβ3 integrins in neonates (Neo.) or adults (Ad.) were analyzed by (A and C) immunofluorescence (N=2), (B and D) Western Blot (N=3) or (E and F) immunohistochemistry (N=2). (A and B) Purified rat brain vessels (BV) were labeled with specific antibodies to (A) α5 integrin to visualize α5β1 expression or (B) β3 integrin to visualize αvβ3 expression. BV were counter-stained using FITC-isolectin B4 and nuclei were labeled with DAPI. Scale bar: 20 µm. Similar contrast adjustment was applied between neonates and adults images. (C and D) 100 µg of rat (C) BV or (D) choroid plexus from 4th ventricle (CP4V) or lateral ventricles (CPLV) were subjected to Western Blot analysis. Actin was used as loading control. (E and F) Sections of human brain tissue were subjected to immunohistochemistry using antibodies to α5 or β3 integrins to visualize α5β1 or αvβ3 respectively, then counterstained with hematoxylin. Representative micrographs of cortex allowing to visualize (E) BV, scale bar: 100 µm or (F) choroid plexuses, scale bar: 50 µm. Arrows indicate BV from choroid vessels displaying positive staining; arrow-heads indicate BV displaying negative staining. Boxed areas correspond to magnification of insets.

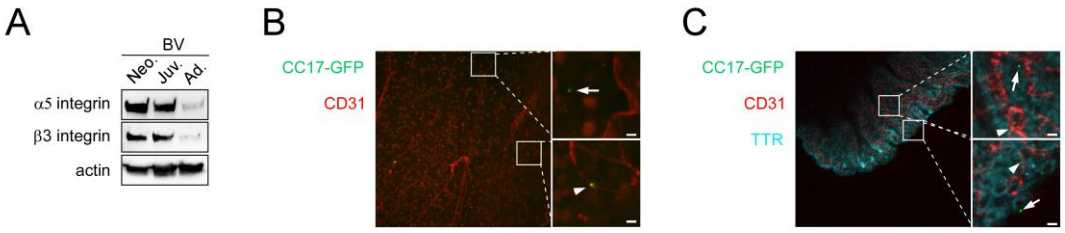

Figure 6: Initial brain penetration of CC17-GBS occurs *via* blood vessels from the cortex and the choroid plexuses. Expression of α5β1 or αvβ3 integrins on purified brain vessels (BV) from neonatal (Neo.), juvenile (Juv.) or adult (Ad.) Balb/C mice was analyzed by Western Blot (N=2) (A) Juvenile mice were infected for 4 h with CC17-GFP strain (green) (N=2). Cerebral blood vessels were stained with CD31 (red) and choroid plexus with anti-TTR (cyan). Cortex (B) and choroid plexuses from the lateral ventricles (C) were examined. CC17-GFP bacteria were found associated with blood vessels (arrowheads) and at distance from blood vessels (arrows). Scale bar = 5 µm.

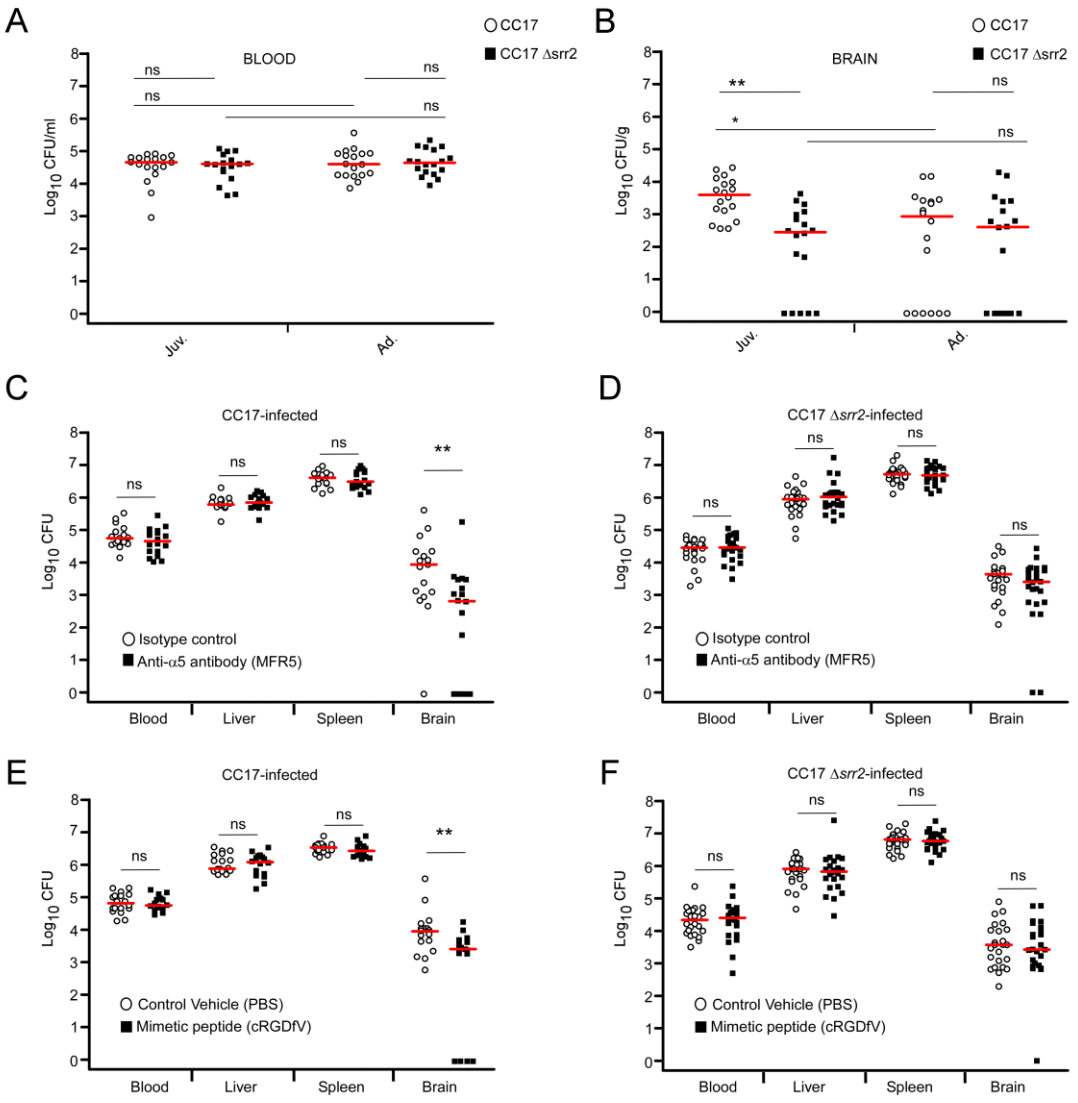

Figure 7: α5β1 and αvβ3 integrins contribute to the juvenile-specific CC17-GBS-elicited meningitis *in vivo*. Juvenile or adult Balb/C mice were infected by intravenous injection with WT CC17 (white circles) or Δ*srr2* mutant (black squares) for 4h. Mice were euthanized and bacterial loads in blood (CFU/ml) (A) and brain (CFU/g) (B) were quantified. Each symbol represents the numeration from one organ from one mouse. Red horizontal lines indicate medians. Statistical analysis: Two-Way ANOVA with Bonferroni's post-test was performed. NS, non-significant; * $p < 0.05$; **, $p < 0.01$.

Juvenile Balb/C mice were pre-treated by (C and D) intravenous injection of 10 µg of anti-α5 antibody to block α5β1 integrin or 10 µg of isotype control, or (E and F) 5 mg/kg of RGDfV mimetic peptide to block αvβ3 or control vehicle (PBS). One hour after pre-treatment, mice were infected by intravenous injection with $2x10^7$ CFU of WT CC17 (C and E) or Δ*srr2* mutant (D and F) for 4 h. Mice were euthanized and bacterial loads in blood (CFU/ml), spleen, liver, and brain (CFU/g) were quantified. Each symbol represents the numeration from one organ from one mouse. White circles: control mice; black squares: treated mice. Red horizontal lines indicate medians. Statistical analysis: Mann-Whitney t test were performed with, NS, non-significant; *, $p < 0.05$; **, $p < 0.01$.